Acoustics interaction in a complex piping network with multiple pulsatile sources

Feroz Ahmed[a], **Ian Eames**[a], **Alireza Azarbadegan**[b], **Emad Moeendarbary**[a]

[a] *Department of Mechanical Engineering, University College London, Torrington Place, London, WC1E 7JE, UK*
[b] *BP Exploration Operating Company Limited, Chertsey Road, Sunbury-on-Thames, Middlesex, TW16 7NL, UK*

Abstract

The interactions between multiple pulsatile sources and the acoustic eigenmodes are analysed to elucidate the influence of source characteristics and contrasting phase differences on the acoustic response in a liquid-filled complex piping network with multiple branches. For illustration, the interactions between two reciprocating pumps operating in a two-branched network are analysed using a one-dimensional linear model. The interactions between sources and acoustic eigenmodes lead to enhanced or suppressed acoustic responses depending on the spatial separation between the sources and their phase differences. The acoustic field measurements from the sweep of driving frequency of a mono-ethylene-glycol (MEG) pump module with two reciprocating pumps in a three-branched network are analysed. The linear model captures the approximate resonance profile of the field measurement data. The presence of plane acoustic wave attenuation in the practical case is influenced by the losses associated with pipe fittings.

Keywords: reciprocating pump, multiple pumps, pulsatile flow, piping network, duct acoustics, acoustic waves, pressure pulsation, hydraulic network, transmission line model

1. Introduction

The presence of multiple acoustic sources in a piping network is a general concern that arises in many industries, such as the HVAC (heating, ventilation and air conditioning) [1], aerospace [2], automotive [1], nuclear [3] and energy sector [4]. This is especially problematic in the energy sector, where the enormous amount of mechanical energy introduced by the reciprocating pumps is transferred into a liquid system that is communicated via acoustic propagation through a piping network. Multiple acoustic sources come with the potential of acoustic resonance that leads to pressure pulse amplification within discrete parts of the network and when coupled with the structural modes can lead to enhanced cavitation and vibration [4, 5, 6] [7, Chapter 5]. Identifying the pump-acoustic resonance behaviour requires a global analysis of the entire piping network, which is challenging especially when we look at the piping networks comprised of multiple branched pipes, a large number of piping discontinuities or pipe fittings (bends, junctions, transitions and valves) and support systems.

Piping systems typically operate with multiple pumps in parallel to increase throughput [8]. The complexities in such systems arise due to each pump generating multiple frequencies (i.e., harmonics), interaction mechanisms between pumps (i.e., contrasting driving frequency and phase differences) and the presence of a long piping network (i.e., eigenmodes) [8, 9]. There are a large number of studies on piping networks with multiple sources in parallel, but they mostly explored the influence of contrasting driving frequency on the structural integrity of the interconnecting

structures [10] and the beating acoustic response in a piping system due to a slight mismatch in the pump driving frequencies [11]. While there has been some attention paid to the piping systems subjected to multiple sources excitation [12, 13, 14, 15, 16], the general influence of their interactions, especially the source characteristics and phase difference, on the acoustic response is scarce [17], and this forms the focus of this work. Here, we applied a general linear acoustic formulation on a liquid-filled complex piping network with multiple pulsatile sources to comprehensively study various contributions to the acoustic resonance. We supported our findings by analysing acoustic field measurements on the off-shore piping network during the pre-commissioning of the high-pressure MEG pump module.

The key physical processes are explained using a one-dimensional linear model (described in §2) with the complexity coming from the steady-state response of a piping network and source characteristics. This is illustrated in §3 through a simplified two-branched piping network that is driven by two pulsatile sources operating in parallel, which is representative of the industrial case. The model is applied to interpret the acoustic responses of field measurements of two high-pressure reciprocating pump configurations with a three-branched piping network in §4, with general conclusions in §5.

2. Mathematical Model

The pump-induced pressure pulsation model is composed of the description of pump flow and acoustic pressure propagation in a piping network.

2.1. Assumptions

The analysis carried out in this study is based on the following assumptions: (i) the dynamics of pump valve is considered ideal, (ii) the fluid is slightly compressible, (iii) the pipe walls are quasi-rigid, (iv) the pipe flow model is linear, (v) the pipe flow model is one-dimensional (1D), and (vi) the energy losses are one-dimensional and quasi-linear. The pump dynamics is discussed in §2.2 and Appendix A, while the pipe flow dynamics is discussed in §2.3 and Appendix B. The pump-related assumptions (i) and pipe flow-related assumptions (ii-vi) are justified in the Appendix C.

2.2. Reciprocating pump – discharge pulsatile flow

For a single pump with N_c chambers driven by a shaft rotating at a frequency f_p, the discharge volume flux (pulsatile flow) due to piston-chamber-valve interaction (see Appendix A.3 and Eq. A.7) is,

$$Q_a = \underbrace{\underbrace{\Big(1-\big(\Delta p\beta r_v + S\big)\Big)}_{\text{volumetric efficiency } \eta_v}\ \underbrace{(A_p l_p f_p N_c)\pi}_{\text{pump displacement}}\ \frac{1}{N_c}\sum_{n=1}^{N_c}}_{\text{actual mean flow } Q_0} \sin\Big(2\pi f_p t + \underbrace{\frac{2\pi}{N_c}(n-1)}_{\text{piston phase } \phi_p}\Big)\cdot F_n(t)\cdot G_n(t), \quad (1)$$

where Q_a is the actual effective flow, A_p the cross-sectional area of a chamber, l_p the stroke length, f_p the pump driving frequency, $\Delta p(= p_d - p_s)$ the differential pressure across discharge and suction valves (where p_d and p_s are discharge and suction pressure, respectively), $\beta(= 1/K)$ the liquid's compressibility factor (where K is the bulk modulus), $r_v(= V_{cd}/V_p)$ the volume ratio (where V_{cd} is the pumping chamber clearance volume and $V_p(= A_p l_p)$ the swept or displacement volume) and S the pump valve slip (or valve loss). The total volume covered by piston/plunger motion is called

as swept volume (V_p), while the the volume of liquid trapped in the chamber space between the suction and discharge valve with the piston/plunger at the end of its discharge stroke is called as clearance volume (V_{cd}) (see Fig. A.6) [18, Chapter 11]. The clearance volume V_{cd} is usually expressed as a percent of pump displacement volume V_p [18, Chapter 11]. The leakage (S) is the consequences of the dynamic delay of valve closure/opening and liquid compressibility in the clearance volume. The typical value of valve loss is $S = 0.02$ [18, Chapter 11] [19] or 0.03 [19]. Each piston/plunger has a phase difference of $2\pi/N_c$ to give a uniform motor torque. The interaction between piston kinematics, chamber fluid dynamics and valve dynamics are associated with the reduction and distortion in the pulsatile flow profile (see Appendix A.3). F_n clips the sine function to account for the discharge flow and G_n accounts for the volumetric efficiency of the pump. Here $F_n = (1/2)(1+\text{sign}(\sin(X_n)))$, $G_n = (1/2)(1+\text{sign}(\sin(X_n-\phi_c)))$, where $X_n = 2\pi f_p t+2\pi(n-1)/N_c$, and ϕ_c is the valve compressibility phase-cut (see Appendix A.3). The phase-cut in the volume flux is related to the volumetric efficiency through $\phi_c = \cos^{-1}(2\eta_v - 1)$ [20]. In the absence of compressibility effects, pump displacement $(A_p l_p f_p N_c)\pi$ is the average volume flux for the pump under incompressible flow conditions [18].

The profiles of a single five-chamber pump is illustrated in terms of Q_a/Q_0 for $\eta_v = 1$ and 0.95 in Fig. 1(a,b). The ϕ_c is as the result of discharge valve delay and compressiblity in the liquid pump system. The Fourier representation of Q_a can be written as,

$$\frac{Q_a(t, f_p)}{\eta_v \pi A_p l_p f_p} = \frac{Q_0}{\eta_v \pi A_p l_p f_p} + \sum_{n=1}^{\infty} A_n \left(\exp(i2\pi f_n t) + \exp(-i2\pi f_n t)\right), \tag{2}$$

where $i = \sqrt{-1}$ and A_n are determined from the Fourier transformation of Eq. 1. The forcing frequencies f_{m_p} of a discharge pulsatile flow is associated with the piston-chamber-valve interaction mechanisms. In a high-pressure pump system, the f_{m_p} can be determined from the combination of volumetric efficiency (η_v), number of chambers (N_c) and pump frequency (f_p) as,

$$f_{m_p} = \begin{cases} 2 \times m_p N_c f_p & \text{for } \eta_v = 1 \\ 1 \times m_p N_c f_p & \text{for } \eta_v < 1 \end{cases}, \tag{3}$$

where f_{m_p} is the pulsatile flow harmonics and $m_p(= 1, 2, 3, ...)$ the pulsatile flow harmonic order or excitation order. In a pump system with high differential pressure Δp, the choice of the multiplier (1 or 2) in Eq. 3 depends on the liquid compressibility (and hence the η_v) in the piston-chamber-valve interaction. The multiplier is 1 and 2 for a pump with compressible ($\eta_v < 1$) and incompressible ($\eta_v = 1$) liquid in chambers, respectively (see Appendix A.3.1 and Fig. A.8).

2.3. Pipe flow model

The acoustic wave propagation in a piping network can be described using the time-domain and frequency-domain analysis. There are a number of models to describe the acoustic propagation in piping networks including finite-element methods [21], finite-difference methods (e.g., Lax-Wendroff [22]), graphical methods (e.g., method of characteristics [23]) and transcendental methods (e.g., transmission line models [22, 23, 24, 25, 26, 27, 28, 29, 30]). Here we choose a standard frequency-domain model for acoustic propagation based on the transfer matrix formulation in the transcendental form that was applied by [22, 23, 25, 26, 30, 31]. This model is based on the linearisation of one-dimensional mass and momentum equations in terms of head-flow (h-Q) representation. We have adopted a similar approach and reformulated the solution in terms of pressure-flow (p-Q) representation in the frequency-domain [27, 28] (see Appendix B). Therefore,

the relationship between the volume flux $\tilde{Q}(i\omega)$ and pressure $\tilde{P}(i\omega)$ at two points of each element (labelled as $j,\ k$) can be written as [28],

$$\begin{pmatrix} \tilde{Q}_{jk,j}(i\omega) \\ -\tilde{Q}_{jk,k}(i\omega) \end{pmatrix} = \underbrace{\begin{pmatrix} Z_{c,jk}^{-1}(i\omega)\cdot\coth\left(\Gamma_{jk}(i\omega)L_{jk}\right) & -Z_{c,jk}^{-1}(i\omega)\cdot\operatorname{csch}\left(\Gamma_{jk}(i\omega)L_{jk}\right) \\ -Z_{c,jk}^{-1}(i\omega)\cdot\operatorname{csch}\left(\Gamma_{jk}(i\omega)L_{jk}\right) & Z_{c,jk}^{-1}(i\omega)\cdot\coth\left(\Gamma_{jk}(i\omega)L_{jk}\right) \end{pmatrix}}_{\boldsymbol{T}(i\omega)} \begin{pmatrix} \tilde{P}_j(i\omega) \\ \tilde{P}_k(i\omega) \end{pmatrix}, \tag{4}$$

where $\tilde{P}$ and $\tilde{Q}$ are the Fourier transformed pressure and volume flux, respectively; j, k the pipe element indices, $\omega(=2\pi f)$ the circular frequency in rad/s, f the frequency of excitation in Hz and L_{jk} the pipe element length (from node j to k). The transmission line parameters, i.e, the propagation operator Γ_{jk} and the characteristic impedance $Z_{c,jk}$ (see Eq. B.10) [28] are,

$$\Gamma_{jk} = \frac{i\omega}{a_0}\sqrt{1+\frac{\pi D}{\rho_0}\frac{\tilde{\bar{\tau}}}{i\omega}}, \qquad Z_{c,jk} = \frac{\rho_0 a_0}{A}\sqrt{1+\frac{\pi D}{\rho_0}\frac{\tilde{\bar{\tau}}}{i\omega}}, \tag{5}$$

where $a_0(=(K/\rho_0)^{1/2})$ is the speed of sound in liquid (see Appendix C.3), ρ_0 the mean (ambient) density of liquid, K the liquid Bulk modulus, $D(=\sqrt{4A/\pi})$ the pipe inner diameter, A the pipe cross-sectional area and $\tilde{\bar{\tau}}$ the Fourier transformation of the linearised approximation of pipe wall shear stress. The pipe wall shear stress (τ) accounts the energy losses through piping network, which can be expressed using convolution operation on Q as $\tau = \bar{\tau} * Q$ (where $\bar{\tau}$ is the linear approximation of shear stress). Using convolution theorem, we can write $\tilde{\bar{\tau}} = \tilde{\tau}/\tilde{Q}$, where $\tilde{\tau}$ is the Fourier transformed pipe wall shear stress.

We have adopted Zielke's [32] and Vardy & Brown's [33, 34, 35, 36] one-dimensional (1D) shear stress decomposition approach for laminar and turbulent pipe flows and expressed the instantaneous pipe wall shear stress (τ) as the combination of quasi-steady component (τ_s) and frequency-dependent unsteady component (τ_u). The τ_s can be modelled using the Darcy-Weisbach equation [22, 23, 37, 38] and the τ_u can be modelled through convolution integral (convolution of local acceleration history with weighting-function) [30, 32, 33, 34, 35, 36, 39] as,

$$\tau(=\tau_s+\tau_u) = \frac{1}{8}\frac{\rho_0\lambda}{A^2}|Q(s,t)|Q(s,t) + \frac{4\rho_0\nu}{DA}\int_0^t W(t-t')\frac{\partial Q(t')}{\partial t}\mathrm{d}t', \tag{6}$$

where λ is the quasi-steady friction loss factor or Darcy-Weisbach friction loss factor, ν the kinematic viscosity, t the time, t' the integration variable with dimension of time, $W(=A_u\cdot\exp(-B_u t)/\sqrt{\pi t})$ the approximate weighting-function, $A_u(=A_u^*(\pi/\nu)^{1/2}D/2)$, $B_u(=B_u^* 4\nu/D^2)$ the unsteady friction convolution parameters, and A_u^* and B_u^* the non-dimensionlised convolution parameters. The τ_s is assumed linear and we can replace $|Q(t)|Q(t)$ in Eq. (6) with $2|Q_0|Q$ for turbulent flows. Therefore, the Fourier transformed pipe wall shear stress ($\tilde{\tau}$) can be written as,

$$\tilde{\bar{\tau}}(=\tilde{\tau}/\tilde{Q}) = \tilde{\bar{\tau}}_s + \tilde{\bar{\tau}}_u = \frac{\rho_0}{\pi D}\left(\frac{\lambda|Q_0|}{DA} + \frac{i\omega 16\nu A_u}{D^2\sqrt{i\omega+B_u}}\right). \tag{7}$$

Note that the term $\lambda|Q_0|/DA$ in Eq. (7) for laminar pipe flows is $\lambda|Q_0|/2DA$. The quasi-steady friction loss factor (λ) is based on the pipe flow regime (Reynolds number $Re_0(=|Q_0|D/A\nu)$) and relative pipe wall roughness (ϵ/D, where ϵ is the absolute roughness). Based on Hagen-Poiseuille and Blasius correlations in smooth-walled pipes [40], the quasi-steady friction terms [38] are,

$$\lambda = \begin{cases} 64/Re_0 & \text{fully-developed laminar pipe flow} \\ 0.3164/Re_0^{0.25} & \text{fully-developed turbulent pipe flow,} \end{cases} \tag{8}$$

respectively. The pipe walls are not always smooth in the practical industrial piping systems. The friction loss factor in rough-walled fully-developed turbulent pipe flow can be described using the Colebrook-White formulation [38] as,

$$\frac{1}{\sqrt{\lambda}} = -2\log\left(\frac{2.51}{Re_0\sqrt{\lambda}} + \frac{\epsilon/D}{3.71}\right). \tag{9}$$

The Blasius and Colebrook-White friction loss factors are accurate for pipe flow with $Re_0 < 10^5$ [40] and $2.5 \times 10^3 \leq Re_0 \leq 10^8$, respectively. The typical value of the roughness of a new commercial steel pipe is $\epsilon = 0.045 \times 10^{-3}$m [41, Chapter 8]. The friction loss factor for smooth and rough-walled pipelines can also be calculated graphically using Moody diagram. To account the losses due to pipe fittings, replace λ with $\lambda + \lambda_{\text{fittings}}$ in Eq. (6), as discussed in the Appendix E (Eq. E.1). Here, λ (Eq. 8, 9) and $\lambda_{\text{fittings}}$ (Appendix E, Eq. E.1) are the quasi-steady friction loss factor for straight and fitting pipes, respectively.

The convolution coefficients (A_u^* and B_u^*) for both smooth and rough-walled pipe flow can be approximated [36] as,

$$\begin{aligned} A_u^* &= \frac{1}{2\sqrt{\pi}} + \frac{\epsilon}{D}\sqrt{Re_0}\left(0.02 + 0.0143\left(\frac{\epsilon}{D}\right)^{-0.44}\right), \\ \frac{B_u^*}{Re_0} &= \frac{Re_0^{0.222}}{6090} + \frac{0.44}{Re_0^{0.278}} + \left(0.0377 + 0.0001\sqrt{\frac{Re_0}{2.04}}\right)\sqrt{\frac{\epsilon}{D}}. \end{aligned} \tag{10}$$

The coefficients A_u^* and B_u^* are accurate in the range $10^3 \leq Re_0 \leq 10^8$ for smooth-walled pipes (with $\epsilon = 0$) and in the range $10^3 \leq Re_0 \leq 10^5$ and $10^{-4} \leq \epsilon/D \leq 10^{-1.5}$ for rough-walled pipes [36].

The field matrices (or local elemental matrices) $\boldsymbol{T}(i\omega)$ (Eq. B.9) link the frequency-dependant complex quantities (acoustic pressure $\tilde{P}$ and volume flux $\tilde{Q}$) at j and k. The global linear transcendental system can be represented as [27],

$$\begin{pmatrix} \tilde{\boldsymbol{Q}}_{\boldsymbol{jk,j}}(i\omega) \\ -\tilde{\boldsymbol{Q}}_{\boldsymbol{jk,k}}(i\omega) \end{pmatrix} = \underbrace{\begin{pmatrix} \boldsymbol{Z_{c,jk}}^{-1}(i\omega)\ \coth \boldsymbol{\Gamma_{jk}}(i\omega) & -\boldsymbol{Z_{c,jk}}^{-1}(i\omega)\ \operatorname{csch} \boldsymbol{\Gamma_{jk}}(i\omega) \\ -\boldsymbol{Z_{c,jk}}^{-1}(i\omega)\ \operatorname{csch} \boldsymbol{\Gamma_{jk}}(i\omega) & \boldsymbol{Z_{c,jk}}^{-1}(i\omega)\ \coth \boldsymbol{\Gamma_{jk}}(i\omega) \end{pmatrix}}_{\boldsymbol{M}(i\omega)} \begin{pmatrix} \tilde{\boldsymbol{P}}_{\boldsymbol{jk,j}}(i\omega) \\ \tilde{\boldsymbol{P}}_{\boldsymbol{jk,k}}(i\omega) \end{pmatrix}. \tag{11}$$

where the bold symbols denote matrices. The global boundary condition of $p = 0$ at an outlet node is applied in Eq. (11) and the boundary conditions at the inlets are set on the left-hand side of Eq. (11). The overall solution is created by looking at each Fourier mode from Eq. (2) inserted at each pump node, and then summing over all the modes.

2.3.1. Limitations

This formulation provides a framework to understand how the interaction between multiple sources influences the acoustic response in a complex piping network. The analysis is valid for plane acoustic wave propagation (see Appendix C.5) in a piping network with straight uniform cross-section (or prismatic) pipe elements. The analysis considers a one-dimensional friction model to account for the plane acoustic wave attenuation in a piping network.

2.4. Acoustic eigenmode analysis

A mismatch in the acoustic impedance generates standing waves (due to wave reflections) in a piping network, which is characterised by an infinite number of acoustic eigenfrequencies. The acoustic eigenmodes of a system (Eq. 11) can be determined by a random forced method [42], where a random forcing is applied to the entire system while maintaining the exit pressure $p = 0$ on the outlet node. This generates a solution,

$$\tilde{\boldsymbol{P}} = \boldsymbol{M}^{-1}(i2\pi f)\boldsymbol{N}(0,1), \tag{12}$$

where $\boldsymbol{N}$ is a vector of normal random distribution. By sweeping across excitation frequencies f and determining the maximum pressure in the system as $\tilde{P}_{max} = \max|\tilde{P}_k|$ (where k is the sweep points), the eigenfrequencies f_{m_a} ($m_a = 1, 2, 3, ...$) and the associated eigenmodes can be determined [42]. The code to solve Eq. (11) was validated against the eigenmodes for an open-closed pipe configuration [43], confirming

$$f_{m_a} = (2m_a - 1)\frac{a_0}{4L} \qquad \text{and} \qquad \tilde{P}_{max} = \cos\left((2m_a - 1)\frac{\pi s}{2L}\right), \tag{13}$$

where s is the pipe streamwise coordinate and L the pipe length. The code was additionally validated with the COMSOL [44] model.

3. Network acoustic response with two sources

We first consider a laminar flow regime in a two-branched piping network driven by two pumps operating in parallel (see Fig. 2a), which provides a framework to understand more complex systems. This section discusses the interaction mechanisms between sources and piping acoustic eigenmodes, taking into account the pump characteristics and pump phase differences.

3.1. Model system

The acoustic system variables are chosen to reflect the typical values of industry (see §4 and Fig. 4) but with certain restrictions; that the pipe fittings (bends, junctions and valves) are neglected and the flow is considered as laminar ($Re_0 = Q_0 D/A\nu = 2000$ with $\nu = 10^{-6}\text{m}^2/\text{s}$, where Re_0 is the Reynolds number, A the pipe cross-sectional area and ν the kinematic viscosity). The topology of a two-branched network consists of two inlet nodes and one outlet node to reflect multiple reciprocating pumps operating in parallel (see Fig. 2a). The system has straight uniform circular cross-section pipes with inner diameter $D = 0.111\text{m}$, outer diameter $D_o = 0.222\text{m}$ and lengths $L_{s(1-2)} = 26.9\text{m}$ (nodes connecting inlet 1 and junction 2), $L_{s(2-3)} = 21.5\text{m}$ (nodes connecting inlet 3 and junction 2) and $L_{s(2-4)} = 51.8\text{m}$ (nodes connecting junction 2 and outlet 4). The acoustic wave speed in a water-filled steel pipe is taken to be $a_0 = 1480\text{m/s}$, which is typical of water in thick stiff pipes. The justification for the choice of the acoustic wave speed is described in the Appendix C.3.

Reciprocating pumps usually consist of an odd number of chambers N_c. Here we considered all parameters based on the field measurement setup (§4.1) except the flow rate. We choose five-chamber pumps driven at a maximum pump frequency of $f_{p,\max} = 5.77\text{Hz}$ that generates a low flux of flow ($Q_0 = 1.74 \times 10^{-4}\text{m}^3/\text{s}$) with $Re_0 = 2000$ (justifying the laminar assumption). The pumps are labelled as pump 1 and 2 in Fig. 2(a). The discharge and suction pressures are $p_d = 78.3\text{MPa}$ and $p_s = 0.7\text{MPa}$, while the clearance volume is $V_{cd} = 0.5V_p$, valve loss is $S = 0.03$ and the stroke length is $l_p = 100 \times 10^{-3}\text{m}$. The net discharge pulsatile flow for a single pump with $\eta_v = 1$ and 0.95

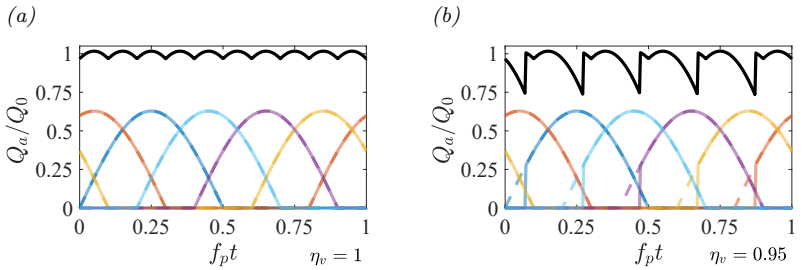

Figure 1. Typical discharge pulsatile flows (black lines) (Eq. 1) from a single five-chamber reciprocating pump under one-complete crank rotation when the volumetric efficiency is (a) $\eta_v = 1$ and (b) 0.95, respectively. The dashed and solid color lines are the individual contributions from each chamber when $\eta_v = 1$ and 0.95, respectively.

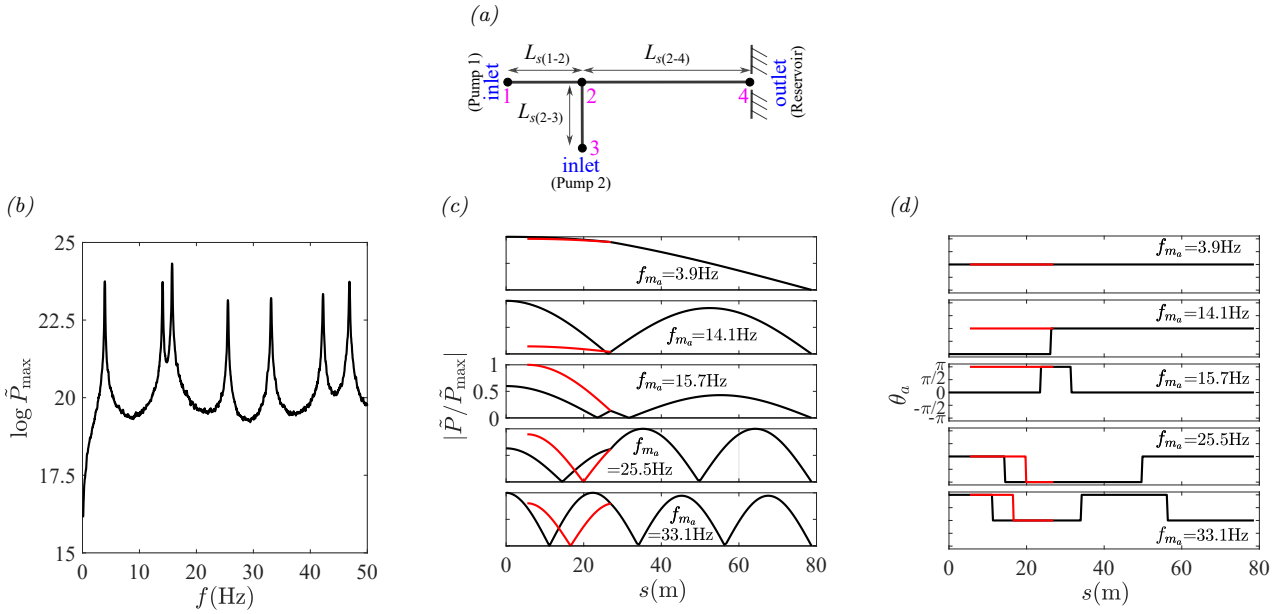

Figure 2. (a) Schematic of a piping network with pulsatile flow sources on two branches. (b) Acoustic eigenfrequencies of a piping network driven by random source excitation. The global maximum pressure within the network is plotted as a function of excitation frequency f. (c,d) First-five normalised acoustic eigenmodes (normalised by their maximum value) and acoustic eigenphases are plotted as a function of spatial coordinate s along a piping network, respectively. The black and red lines correspond to the line from pump 1 (node 1) to exit (node 4) and pump 2 (node 3) to mainline junction (node 2), respectively.

are shown in Fig. 1. The pulsatile flow profile at $\eta_v = 0.95$ (see Fig. 1b) is established based on the manufacturer's data of pump, which were used during the pre-commissioning of MEG pumps.

As with the presence of large differential pressure, $\Delta p(= p_d - p_s) = 77.6$MPa, across the pump with $\eta_v = 0.95$, the fluid compressibility, leakage and valve timings lead to a delay in the outflow and a jump-discontinuity in the volume flux [18, Chapter 2] [8, 20, 45, 46, 47] (expressed in terms of phase-cut ϕ_c), as shown in Fig. 1(b). The mechanism of flow jump-discontinuity is discussed in the Appendix A (see Fig. A.7a). The pulsation harmonics are determined from Eq. (3), which depends on Δp across the pump (see Fig. A.8). When the chamber liquid is incompressible in a high-pressure pump, the volume flux tends to be symmetrical (see Fig. 1a and A.8a). When the chamber liquid is compressible in a high-pressure pump, the symmetry of the volume flux is broken by the jump in Q_a (see Fig. 1b and A.8b,c). For pulsatile flow with $\eta_v = 1$ and $\eta_v = 0.95$, the fundamental excitation frequency (Eq. 3 with $m_p = 1$) becomes $2 \times N_c f_p = 2 \times 5 \times 5.77 = 57.70$Hz and $1 \times N_c f_p = 1 \times 5 \times 5.77 = 28.85$Hz, respectively (see Fig. A.8a,b). The successive pulsatile

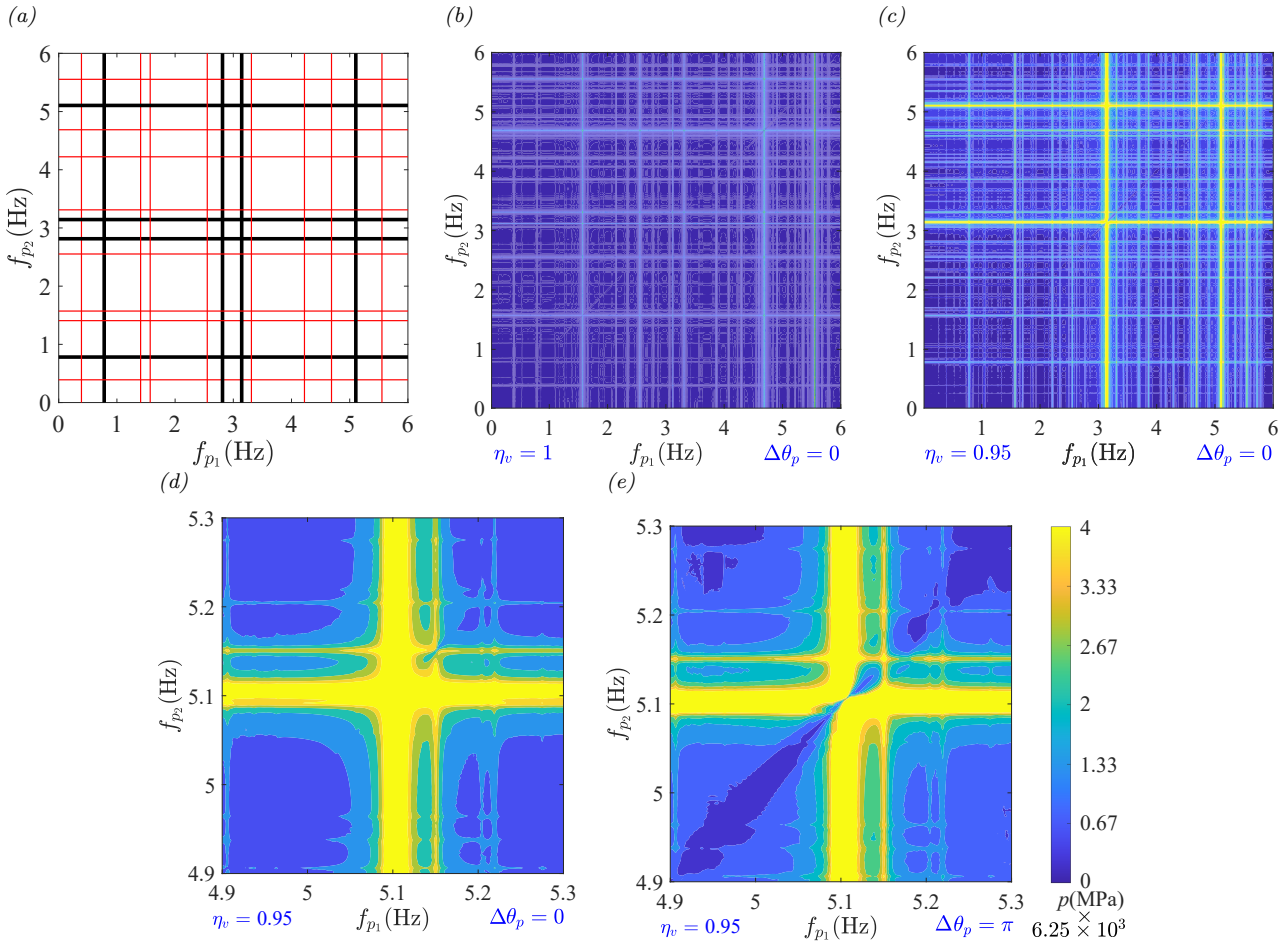

Figure 3. (a) Potential occurrence of acoustic resonance in a piping network due to pumps with incompressible ($\eta_v = 1$) ($f_p = f_{m_a}/10$; red lines) and compressible ($\eta_v < 1$) ($f_p = f_{m_a}/5$; black lines) liquid in the chambers. (b,c) Magnitude of normalised acoustic pressure at node 3 when the driving frequency of pumps were varied from 0 to 6Hz for pulsatile flows with volumetric efficiency $\eta_v = 1$ and 0.95, respectively. Here the frequency of pump 1 and 2 are set equal to f_{p_1} and f_{p_2}, respectively. (d,e) Zoomed-in regions showing the influence of pump phase difference ($\Delta\theta_p = 0$ and $\Delta\theta_p = \pi$, respectively) on the acoustic response for pulsatile flow with $\eta_v = 0.95$.

flow harmonics are then multiple of harmonic order $m_p(= 2, 3, 4...)$ (see Eq. 3).

Acoustic eigenmode analysis of a piping network (see Fig 2a) is conducted using Eq. (12) to characterise the standing wave patterns in a piping network. This is expressed in terms of eigenfrequencies, eigenmodes and eigenphases (see Fig 2b,c and d, respectively). The phase differences exist between the driving flows and between the acoustic eigenmodes of piping branches. In our study, $\Delta\theta_p(= |\theta_{p_2} - \theta_{p_1}|)$ represents the phase difference between pump 1 (node 1) and pump 2 (node 3), and $\Delta\theta_a(= |\theta_{a_3} - \theta_{a_1}|)$ represents the phase difference between the acoustic eigenmodes of two branches ($L_{s(1-2)}$ and $L_{s(2-3)}$). The $\Delta\theta_p$ is due to the relative delay in the starting operation of each pump and the $\Delta\theta_a$ is due to the spatial variation in branch lengths. The two extreme values of $\Delta\theta_p$ and $\Delta\theta_a$ are 0 (in-phase) and π (out-of-phase). The acoustic eigenphase differences ($\Delta\theta_a$) between two branches (at node 1 and 3) are 0, π, π, 0 and 0 for the first ($f_{m_a} = 3.9$Hz), second ($f_{m_a} = 14.1$Hz), third ($f_{m_a} = 15.7$Hz), forth ($f_{m_a} = 25.5$Hz) and fifth ($f_{m_a} = 33.1$Hz) modes, respectively (see Fig 2d).

3.2. Potential for acoustic resonance

The acoustic response depends on the pulsatile flow harmonics (f_{m_p}) (Eq. 3) of pumps and the acoustic eigenfrequencies (f_{m_a}) (Eq. 12) of a piping network. Resonance occurs when one of the pulsatile flow harmonics (Eq. 3) coincides (or is close to, within 20% [5]) with one of the acoustic eigenfrequencies (see Fig. 2*b,c* and *d*) as $f_p = f_{m_a}/\big((1 \text{ or } 2) \times m_p N_c\big)$. Fig. 3(*a*) shows the potential occurrence of the acoustic resonance due to liquid compressibility in the chamber of high-pressure pumps. The coincidence of the fundamental excitation frequency of pulsatile flow ($m_p = 1$) of five chamber ($N_c = 5$) pumps with the acoustic eigenmodes of a piping network is shown with black lines ($f_p = f_{m_a}/5$) and red lines ($f_p = f_{m_a}/10$) for pump with compressible ($\eta_v < 1$) and incompressible ($\eta_v = 1$) liquid in the chambers, respectively. Therefore, the potential acoustic responses are the red and black lines for pulsatile flows with $\eta_v = 1$ and $\eta_v = 0.95$, respectively.

3.3. Source-acoustic interactions

When the pumps are driven in phase ($\Delta\theta_p = 0$) under the sweep of driving frequencies, we obtained the dominant acoustic responses for $\eta_v = 1$ and $\eta_v = 0.95$, (see Fig. 3*b,c*, respectively). These are consistent with the red and black lines of Fig. 3(*a*). The dominant acoustic responses in a network with pulsatile flow of $\eta_v = 1$ occur when both pumps ($f_{p_1} = f_{p_2}$) are operating at 1.57, 2.55, 3.31, 4.69 and 5.55Hz (see Fig. 3*b*). These frequencies are consistent with the red lines in Fig. 3(*a*). Similarly, for pulsatile flow with $\eta_v = 0.95$, the dominant acoustic responses are consistent with the black lines in Fig. 3(*a*), for example, 3.14 and 5.1Hz (see Fig. 3*c*). The relatively large network acoustic response due to pulsatile flows with $\eta_v = 0.95$ compared to the flows with $\eta_v = 1$ is anticipated from the presence of large variation in the volume flux (see Fig. 1*a,b*).

When the pumps are operating at the same driving frequency ($f_{p_1} = f_{p_2}$), the resonance state of a piping network depends on the interplay of the phase difference between driving flows ($\Delta\theta_p$) and phase difference between the eigenmodes of piping branches ($\Delta\theta_a$). Fig. 3(*d,e*) contrasts the influence of $\Delta\theta_p$ on the network acoustic responses for pulsatile flow with $\eta_v = 0.95$. The constructive interference occurs when both $\Delta\theta_p$ and $\Delta\theta_a$ are in-phase ($\Delta\theta_p = 0$ and $\Delta\theta_a = 0$) or out-of-phase ($\Delta\theta_p = \pi$ and $\Delta\theta_a = \pi$). The destructive interference occurs when $\Delta\theta_p$ and $\Delta\theta_a$ are opposite ($\Delta\theta_p = 0$ and $\Delta\theta_a = \pi$, or $\Delta\theta_p = \pi$ and $\Delta\theta_a = 0$). The constructive interference leads to an enhancement in the acoustic pressure at resonance state around $f_p = 5.1$Hz (see Fig. 3*d*). This is attributed to the interaction of in-phase pump operation ($\Delta\theta_p = 0$) and in-phase acoustic eigenmodes ($\Delta\theta_a = 0$) (see the fourth acoustic eigenmode $f_{m_a} = 25.5$Hz in Fig. 2*d*). Similarly, the destructive interference leads to suppressed acoustic pressure and is associated to the interaction of out-of-phase pump operation ($\Delta\theta_p = \pi$) and in-phase acoustic eigenmodes ($\Delta\theta_a = 0$) (see Fig. 3*e*).

4. Application to field observations

The analysis is now applied in the turbulent flow regime to interpret the field measurements on a three-branched piping network with two pumps operating in parallel (see Fig. 4).

4.1. Diagnostic setup

In this study, mono-ethylene-glycol (MEG) pump modules consist of three parallel high-pressure reciprocating plunger pumps connected to a complex piping network (see Fig. 4*a*). The use of two or more pumps is usual [8, 45, 48] – with one pump being redundant except during the

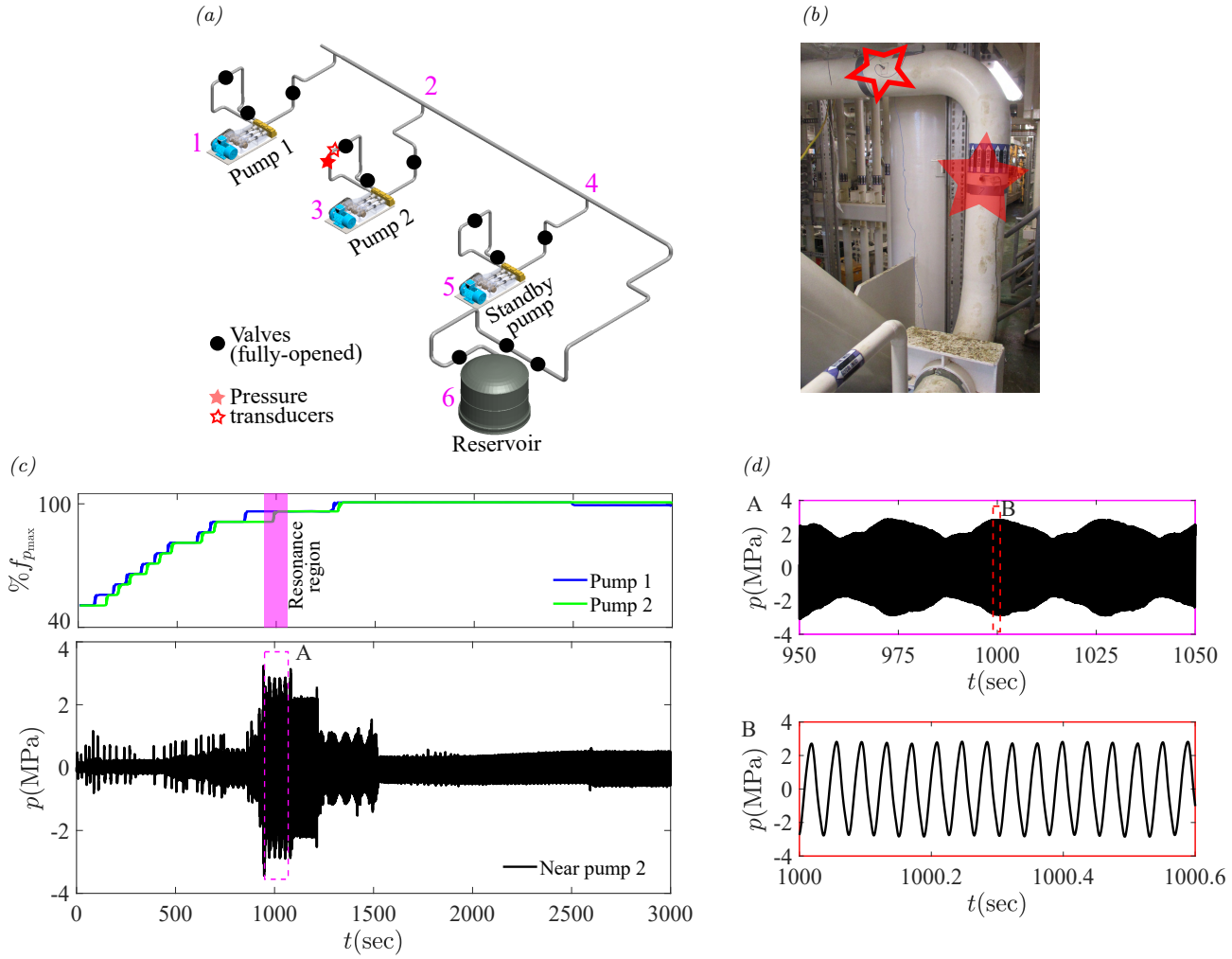

Figure 4. (a) Three-dimensional layout of MEG pump-piping system used in the offshore field study. The pump system consists of three high-pressure five-chamber reciprocating plunger pumps with a volumetric efficiency of $\eta_v = 0.95$. (b) Snapshot of piping installation with pressure transducers near pump 2. The pressure transducers are marked as red stars. The data of pressure transducer with closed red star-maker (in a and b) is presented in this study. (c) Acoustic pressure envelope (bottom panel) captured near pump 2 during pump sweep test (top panel). The top and bottom panel shows the plot of pump driving frequency (f_p) and acoustic pressure (p) over time, respectively. The pump speed is varied from $0.5 \times f_{p,\max}$ to $f_{p,\max}$. (d) Zoomed-in regions of acoustic response at resonance condition showing beating phenomenon.

period when one pump is being serviced. The simplified network representation of the MEG pump-piping modules is shown in Fig. 5a. The spatial dimensions of a network are: (a) pipe lengths $L_{s(1-2)} = 26.9\text{m}$, $L_{s(2-3)} = 21.5\text{m}$, $L_{s(2-4)} = 12.1\text{m}$, $L_{s(4-5)} = 20.6\text{m}$ and $L_{s(4-6)} = 39.7\text{m}$, (b) pipe diameters $D_{(1-2)} = 0.086\text{m}, D_{o(1-2)} = 0.168\text{m}$, $D_{(2-3)} = 0.086\text{m}, D_{o(2-3)} = 0.168\text{m}$, $D_{(2-4)} = 0.111\text{m}, D_{o(2-4)} = 0.22\text{m}$, $D_{(4-5)} = 0.086\text{m}, D_{o(4-5)} = 0.168\text{m}$ and $D_{(4-6)} = 0.111\text{m}, D_{o(4-6)} = 0.22\text{m}$ (where D and D_o are inner and outer diameters). The pipe fittings (bends, junctions and valves) are included into the friction model (see Eq. 7) through equivalent length and resistance coefficient methods (see Eq. E.1 in Appendix E) – expressed in terms of total loss factor $(\lambda + \lambda_{\text{fittings}})$, where λ and $\lambda_{\text{fittings}}$ are quasi-steady loss factor associated with straight and fitting pipes. Only pump 1 (at node 1) and pump 2 (at node 3) are under operation and the branch (node 4-5) connected to the pump 3 (at node 5) act as a dead-leg. Each pump with $\eta_v = 0.95$ generates high flux of flows ($Q_0 = 6.11 \times 10^{-3}\text{m}^3/\text{s}$ and $Re_0 = 9.9 \times 10^4$).

The measurements were conducted during the pre-commissioning stage of the project on a piping network with the fully-opened configuration of valves. During the pre-commissioning of pump modules, sweep tests were conducted with water to study the influence of multiple pump interactions on the network acoustic response. This was achieved by varying the driving frequency of pump 1 and 2 from $0.5 \times f_{p,\max}$ to $f_{p,\max}$ (where $f_{p,\max} = 5.77$Hz) (see the top panel in Fig. 4*c*). The acoustic pressures were captured at a number of locations using pressure transducers (KISTLER type 6005). In our study, we only focus on the data reported near pump 2 (see closed red star marker in Fig. 4*a,b*), which is shown in the bottom panel of Fig. 4*c*. The data acquired with the 24-bit data acquisition system (DAQ) were sampled at 2048Hz.

4.2. Results

Acoustic measurement near pump 2 based on the sweep test is shown in Fig. 4(*c*), The acoustic pressure is greatly enhanced due to resonance (at $f_p (= 0.91 \times f_{p,\max}) = 5.25$Hz) in the range $900 < t < 1100$s. The interactions of pumps operating at very close driving frequencies ($f_p = 5.25$Hz) generates beating phenomenon with beat frequency of $\Delta f (= f_{p1} - f_{p2}) = 0.04$Hz (see Fig. 4*d*).

The acoustic eigenfrequencies, eigenmodes and eigenphases of a simplified network (see Fig. 5*a*) were calculated using a linear model (Eq. 11) in the absence of fitting losses ($\lambda_{\text{fittings}} = 0$ in Eq. E.1 and 7), as shown in Fig. 5(*b, c* and *d*), respectively. To investigate the influence of piping topology, we first analysed the real network (three-dimensional topology) (see Fig. 4*a*) using COMSOL [44] and the simplified network (two-dimensional topology) (see Fig. 5*a*) in the absence of fitting losses using a linear model (Eq. 11). The similarity of eigenmodes in the COMSOL (to solve Fig. 4*a*) and linear model (to solve Fig. 5*a*) confirms that the plane acoustic wave propagation is independent of piping topology.

We also found out that the response of a simplified network (see Fig. 5*a*) in the absence of fitting losses, considering the turbulent pulsatile pipe flows are approximately similar to the response due to the laminar pulsatile pipe flows. The quasi-laminar characteristics can be anticipated from the presence of a relatively thin acoustic boundary layer compared to the turbulent viscous sublayer in the pulsatile pipe flows (see Appendix D).

To understand the influence of fitting losses on the acoustic response of a piping network (see Fig. 5*a*), we incorporated the fitting friction model (Eq. E.1 into Eq. 7) into the propagation operator (Γ_{jk}) and characteristic impedance (Z_{jk}) (Eq. 5) of a linear acoustic model (Eq. 11). The method used to integrate fitting losses into a linear acoustic model and the influence of fitting losses on the acoustic responses are discussed in the Appendix E (see Fig. E.9). Fig. 5(*e*) shows the effect of fitting losses on the network acoustic response with pumps operating in phase ($\Delta\theta_p = 0$). Two cases are considered: (a) a simplified network (see Fig. 5*a*) without fitting losses ($\lambda_{\text{fittings}} = 0$) and (b) a simplified network (see Fig. 5*a*) with fitting losses ($\lambda + \lambda_{\text{fittings}}$). Here, the quasi-steady fitting loss factor is $\lambda_{\text{fittings}} = \lambda_{\text{fittings,bends}} + \lambda_{\text{fittings,junctions}} + \lambda_{\text{fittings,valves}}$ (see Table E.1 and Fig. E.9). The significant difference in acoustic pressure profiles between the linear model without and with fitting losses implicates the role of plane acoustic wave propagation associated with pipe fittings (see Fig. E.9). The four major differences observed while comparing the linear model with and without fitting losses are: (a) the slight decrease in resonance frequencies, (b) the smearing (or widening) of resonance peaks (c) the reduction in peak amplitudes and (d) the annihilation of some of the peaks.

The enhancement and suppression of acoustic resonance depend on the phase interactions between pumps ($\Delta\theta_p$) and acoustic eigenmodes ($\Delta\theta_a$) of a piping network. The acoustic eigenphases (θ_a) are presented in Fig. 5(*d*), where the first ($f_{m_a} = 4.3$Hz), second ($f_{m_a} = 12.7$Hz), forth

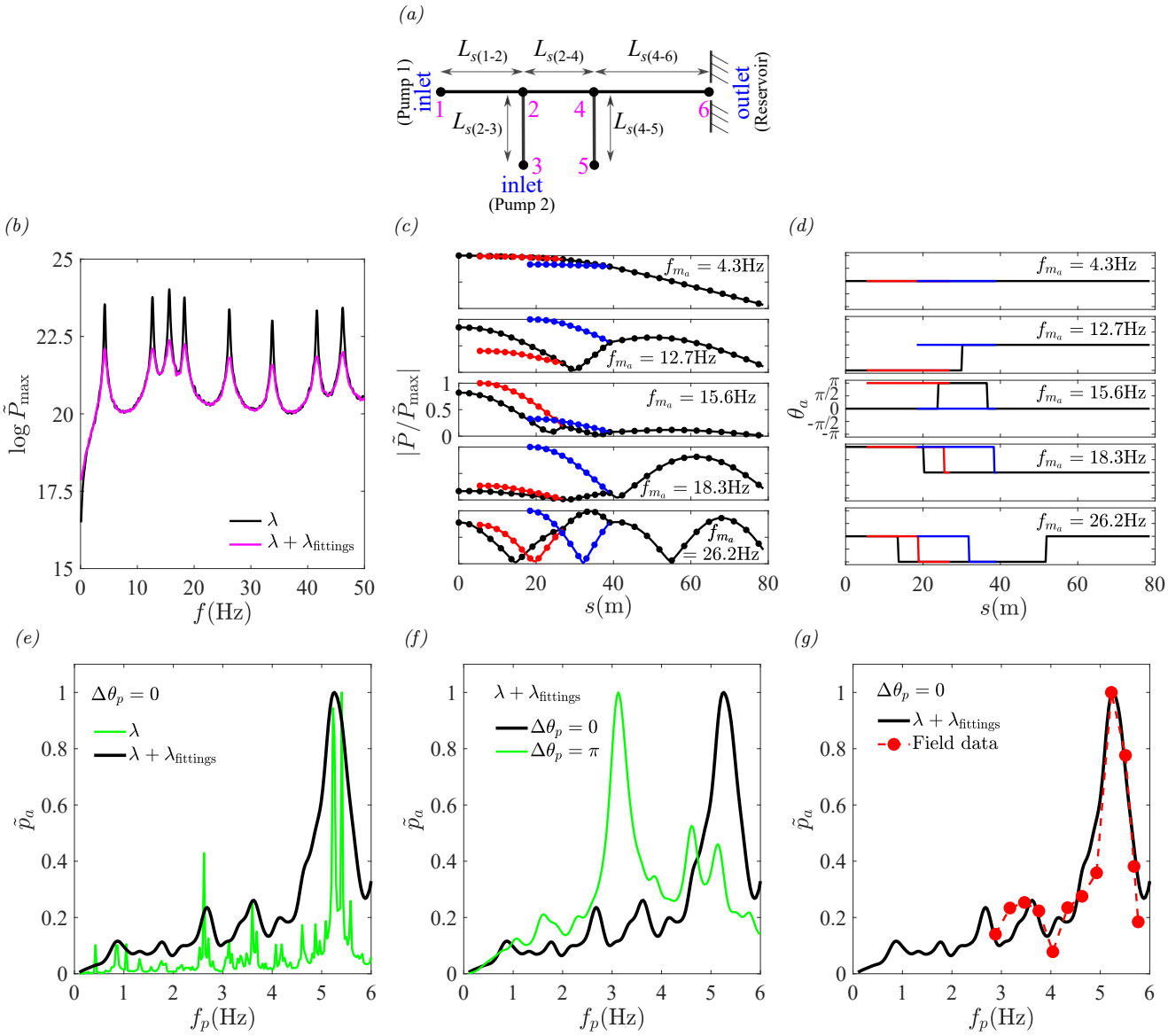

Figure 5. (a) Simplified network representation of the offshore pump-piping system (see Fig. 4a). (b) Comparison of acoustic eigenfrequencies of a piping network driven by random source excitation. Two cases are considered for losses (Eq. 7) in a piping network in terms of friction loss factor (λ) (Eq. 8) – without fitting losses ($\lambda_{\text{fittings}} = 0$) and with fitting losses ($\lambda + \lambda_{\text{fittings}}$) (Eq. E.1). ($c$) Comparison of normalised acoustic eigenmodes between linear model (solid lines) (Eq. 11) and COMSOL model [44] (closed circular makers) in the absence of fitting losses. (d) Acoustic eigenphases (θ_a) plotted along a piping network. The black, red and blue lines correspond to the line from pump 1 (node 1) to exit (node 6), pump 2 (node 3) to mainline junction (node 2) and pump 3 (node 5) to mainline junction (node 4), respectively. The acoustic eigenphase differences ($\Delta\theta_a$) between two branches ($L_{s(1-2)}$ and $L_{s(2-3)}$) are 0, 0, π, 0 and 0 for first ($f_{m_a} = 4.3$Hz), second ($f_{m_a} = 12.7$Hz), third ($f_{m_a} = 15.6$Hz), forth ($f_{m_a} = 18.3$Hz) and fifth ($f_{m_a} = 26.2$Hz) modes, respectively. (e) Comparison of acoustic pressure calculated using a linear model without fitting losses ($\lambda_{\text{fittings}} = 0$) and with fittings losses ($\lambda + \lambda_{\text{fittings}}$) at pump phase of $\Delta\theta_p = 0$. (f) Influence of pump phase difference ($\Delta\theta_p$) on the acoustic resonance for a piping network under the consideration of fitting losses ($\lambda + \lambda_{\text{fittings}}$). ($g$) Comparison of acoustic pressure calculated using a linear model with fitting losses ($\lambda + \lambda_{\text{fittings}}$) and field data. In e, f and g, the pressure p_a is normalised by their maximum values.

($f_{m_a} = 18.3$Hz) and fifth ($f_{m_a} = 26.2$Hz) modes are in-phase ($\Delta\theta_a = 0$), while the third mode ($f_{m_a} = 15.6$Hz) is out-of-phase ($\Delta\theta_a = \pi$) near pump 2 (node 2-3). Figure 5(f) shows how the

pump phase differences ($\Delta\theta_p$) lead to constructive/destructive interferences, which is dependent on the spatial separation between pumps and hence the acoustic eigenphase differences ($\Delta\theta_a$). For $\Delta\theta_p = 0$, the constructive resonance occurs when one of the pump harmonics coincides with the in-phase acoustic eigenmodes ($\Delta\theta_a = 0$). While the destructive resonance is due to the coincidence with the out-of-phase acoustic eigenmodes ($\Delta\theta_a = \pi$). When the pumps are operating in-phase ($\Delta\theta_p = 0$), the acoustic response at $f_p(= 0.91 \times f_{p,\max}) = 5.25$Hz and $f_p(= 0.52 \times f_{p,\max}) = 3$Hz are enhanced and suppressed, respectively. The acoustic enhancement at $f_p = 5.25$Hz is due to the interaction of in-phase pump phase difference ($\Delta\theta_p = 0$) with the in-phase fifth acoustic eigenphase difference ($\Delta\theta_a = 0$ at $f_{m_a} = 26.2$Hz) (see Fig. 5d). The acoustic suppression at $f_p = 3$Hz is due to the interaction of in-phase pump phase difference ($\Delta\theta_p = 0$) with the out-of-phase third acoustic eigenphase difference ($\Delta\theta_a = \pi$ at $f_{m_a} = 15.6$Hz) (see Fig. 5d). Similar interaction mechanism is also observed for pumps operating with out-of-phase ($\Delta\theta_p = \pi$). We analysed the source-acoustic interaction under two extreme pump phase difference operations, i.e., in-phase ($\Delta\theta_p = 0$) and out-of-phase ($\Delta\theta_p = \pi$). In practical systems, the pumps can operate over a wide range of $\Delta\theta_p$ between 0 and π, and hence the piping network can undergo a wide range of acoustic interference.

Fig. 5(g) shows the comparison of acoustic pressure between the field measurement and a linear model (with the inclusion of fitting losses). The linear model captures the resonance profile of field measurement with a good approximation. The analysis neglects the flow interactions between closely-spaced multiple pipe fittings. Only the isolated fitting losses are incorporated into the linear model to account for acoustic attenuation due to pipe fittings. We speculate that one of the major reasons for the slight differences between the measurement and linear model is due to the influence of three-dimensional flow interactions between multiple closely-spaced pipe fittings.

5. Summary and Conclusion

The study used a simplified yet effective one-dimensional linear model to highlight various contributions to the acoustic resonance in a liquid-filled complex piping network with multiple pulsatile sources. While the acoustic resonance in a complex piping network may appear to be simple, the complexity arises due to the differential pressure across pumps, the interaction between driving flows and the acoustic eigenmodes of networks with multiple branches. We investigated the two-branched network (see Fig. 2a) and three-branched network (see Fig. 5a), which are drawn from a practical case during a pre-commissioning process (see Fig. 4a). These networks are driven by multiple high-pressure multi-chamber reciprocating plunger pumps. The linear model first explained the source-acoustic interactions in a two-branched network under the assumption of negligible fitting losses in a laminar flow regime. The network acoustic resonance is found to be driven by the chamber's liquid compressibility in high-pressure pumps. The enhancement and suppression of acoustic response have been found to be driven by the interactions between pump phase difference and acoustic eigenmodes phases (see Fig. 3 and 5). The observed experimental acoustic response can be simply captured by considering the fitting losses (see Eq. E.1 and Fig. E.9) to account for the plane acoustic wave attenuation through a piping network (see Fig. 5g). The effect of transient phenomena can be dealt with in the future.

Acknowledgement

A.A. acknowledges the support of Geoff Evans (BP) for this collaborative project. E.M. is grateful for financial support from the Biotechnology and Biological Sciences Research Council (BB/V001418/1) and Engineering and Physical Research Council (EP/W009889/1).

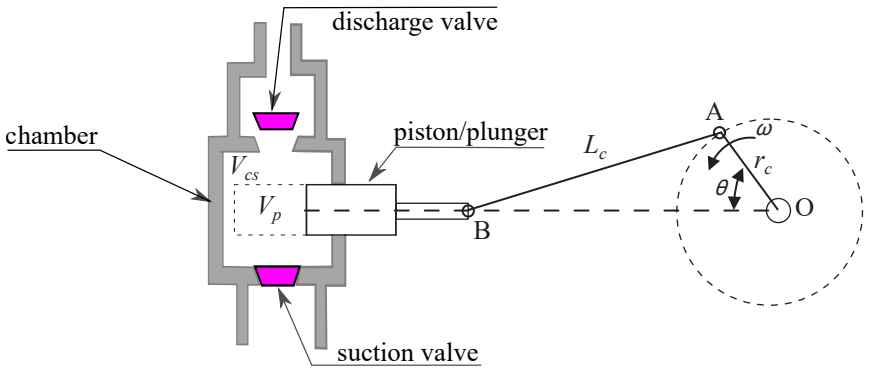

Figure A.6. Schematic showing the general piston slider-crank mechanism during the discharge stroke. *O-A* is the crank link (with radius r_c), *A-B* the connecting rod link (with length L_c), $\omega(= 2\pi f_p)$ the crank angular velocity, $\theta(= 2\pi f_p t)$ the crank angular position, V_p the piston/plunger displacement (or swept or displacement volume), V_{cs} and $V_{cd}(= V_{cs} - V_p)$ the chamber volume between suction and discharge valve with the piston/plunger at the end of suction and discharge stroke, respectively. V_{cd} is also called clearance volume.

Funding

This work was supported by the UK Engineering and Physical Science Research Council (EPSRC) and British Petroleum (BP) through Industrial Cooperative Awards in Science & Technology (iCASE) [Grant number EP/S513726/1, PhD studentship project reference number 2309782].

CRediT author statement

Feroz Ahmed: Conceptualisation; Methodology; Modeling; Software; Investigation; Validation; Visualisation; Writing – original draft; Manuscript revision. **Ian Eames**: Conceptualisation; Methodology; Investigation; Writing - review editing; Supervision. I.E. Wrote and validated software / programmes for solving Eq. 2 and 11 for a general pipe network. Software. **Emad Moeendarbary**: Funding acquisition; Writing - review editing; Supervision; Project administration. **Alireza Azabadegan**: Validation; Supervision; Resources

Declaration of interests

The authors report no conflict of interest.

Appendix A. Pulsatile flow

A reciprocating pump, driven by a common crankshaft, consists of multiple chambers with pistons/plungers and spring-loaded valves to create a unidirectional flow [49]. The nature of actual discharge flow is influenced by the interaction of piston/plunger motion (piston kinematics), chamber incompressible or compressible motion (chamber fluid dynamics) and valve motion (valve dynamics) [49].

Appendix A.1. Piston kinematics

Fig. A.6 shows the slider-crank mechanism in a single-chamber single-acting reciprocating piston/plunger pump. The rate at which the fluid is displaced due to the linear motion of piston/plunger can be characterised by the instantaneous piston velocity, expressed as [18, 47],

$$v_p = 2\pi f_p \cdot r_c \cdot \sin(2\pi f_p t) \cdot \left(1 + \frac{r_c}{L_c} \frac{\cos(2\pi f_p t)}{\sqrt{1 - \left(r_c/L_c\right)^2 \sin^2(2\pi f_p t)}}\right), \tag{A.1}$$

where r_c is the crank radius in meters, L_c the connecting rod length in meters, f_p the pump driving frequency in Hz. We ignored the effect of r_c/L_c in our study, as the connecting rod length is significantly larger than the crank radius (i.e., $r_c/L_c \simeq 0$) in industrial pumps. On substituting $2r_c = l_p$ (where l_p is the stroke length in meters), the instantaneous piston velocity becomes,

$$v_p \simeq l_p f_p \pi \cdot \sin(2\pi f_p t). \tag{A.2}$$

Appendix A.2. Chamber fluid dynamics

The piston-chamber interaction (i.e., the motion of piston/plunger in a liquid chamber) generates volume flux as,

$$Q_{pc,s} = A_p v_p\{2\pi f_p t\} \simeq (A_p l_p f_p)\pi \cdot \sin(2\pi f_p t), \tag{A.3}$$

where the subscript pc, s stands for piston-chamber interaction in a single piston-chamber arrangement, A_p the piston area and $(A_p l_p f_p)\pi$ the pump displacement (or kinematic displacement or theoretical liquid displacement). The real pump consists of multiple piston-chamber arrangements with relative phase difference between pistons as $2\pi/N_c$ (where N_c is the number of piston-chamber arrangements). The interaction between chambers generate a net volume flux (pulsatile flow) as,

$$Q_{pc,m} = A_p \sum_{n=1}^{N_c} v_p\{2\pi f_p t + \phi_p\} = (A_p l_p f_p)\pi \sum_{n=1}^{N_c} \sin\Big(2\pi f_p t + \underbrace{\frac{2\pi}{N_c}(n-1)}_{\text{piston phase } \phi_p}\Big), \tag{A.4}$$

where the subscript pc, m stands for piston-chamber interaction in multiple piston-chamber arrangements. The $Q_{pc,m}$ is the idealised effective pulsatile flow from perfect pump with multi-chambers, where the occurence of leakage (slip) while displacing incompressible liquid is neglected [46] (see Fig. 1*a* and A.8*a*).

Appendix A.3. Valve dynamics

The actual discharge volume flux (or real fluid displacement) Q_0 from a high-pressure reciprocating pump is always less than the geometrical and kinematic displacement (or theoretical fluid displacement) $Q_{0t}(= A_p l_p f_p \pi)$, i.e., $Q_0 < Q_{0t}$ and $\eta_v(= Q_0/Q_{0t}) < 1$, where η_v is the volumetric efficiency. The major parameters that reduce the η_v under high differential pressure (Δp) across pumps are: (a) the compressible liquid ($\beta = 1/K$) trapped in the chambers at the end of discharge stroke and (b) the leakage (or slip S) through valves [18, 20]. The volumetric efficiency [18, 19, 45] thus can be expressed as,

$$\eta_v = 1 - \Big(\Delta p \beta r_v + S\Big), \tag{A.5}$$

The labelling of variables in Eq. (A.5) is discussed in §2.2. The piston/plunger requires an additional motion while decompressing the trapped liquid before the suction valve can open during the suction stroke [47]. A similar additional motion is also required during the discharge stroke while compressing the trapped liquid before the discharge valve can open. The compression and decompression lead to a sudden drop and rise in the suction and discharge pressures, respectively. Therefore, the additional motion due to the interaction between the valve delay motion and liquid

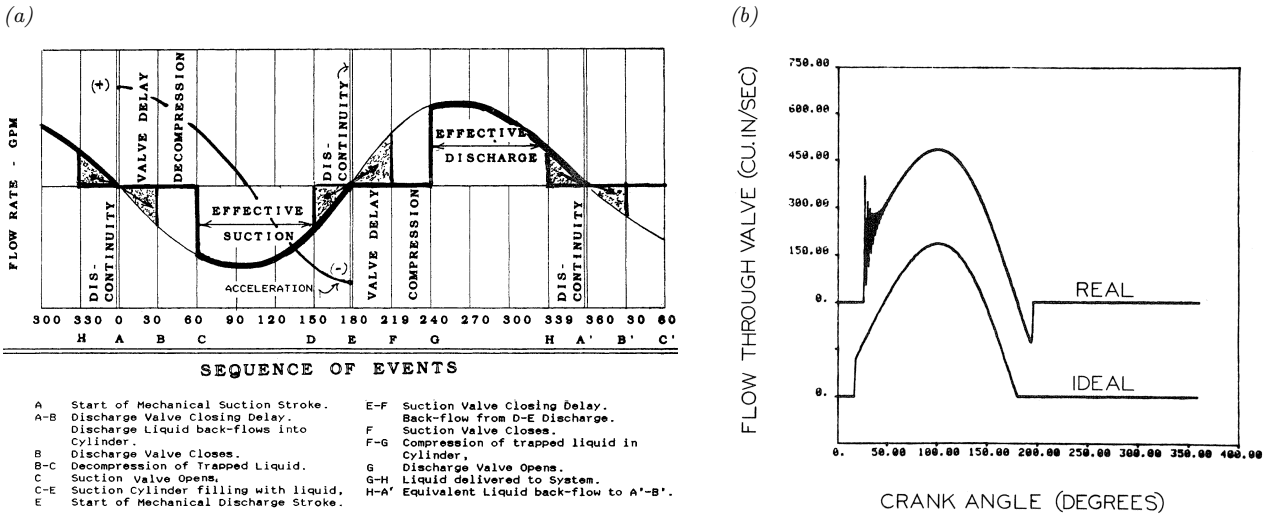

Figure A.7. (a) Mechanism of jump-discontinuity in the discharge pulsatile flow due to the dynamic delay of pump valve closure or opening during piston-chamber-valve interaction [18, Chapter 2, Fig. 2.1A]. (b) Comparison of pulsatile flows from pumps with ideal and real valve dynamics [8, Fig. 4]. The real valve dynamics are associated with an overshoot at the jump-discontinuity. The overshoot is suppressed by the ideal valve assumption.

compressibility leads to the loss in the effective piston/plunger motion (see Fig. A.7). The additional motion (or the loss in volume flux) can be described in terms of phase-cut [20] as,

$$\phi_c = \cos^{-1}(2\eta_v - 1). \tag{A.6}$$

Based on the dynamics of valve motion (ideal or actual), the two types of distorted pulsatile flow associated with the piston-chamber-valve interactions are: (a) flow with jump-discontinuity under ideal valve dynamics [18, 45] (see Fig. A.7b, 1b and A.8b,c) and (b) flow with transient oscillation at the jump-discontinuity under actual valve dynamics [47] (see Fig. A.7b). The ideal valve dynamics assumption means that the valve can open and close instantly and perfectly. We assumed valve motion as the perfect step-like profile. The effective discharge flow due to ideal valve dynamics without delay (see Fig. 1a) and with delay (see Fig. 1b) are considered in this study.

Appendix A.3.1. Effective discharge pulsatile flow

The reciprocating pump generates a wide range of discharge pulsatile flow patterns based on the interaction of piston kinematics, chamber fluid dynamics and valve dynamics. The general effective discharge pulsatile flow due to piston-chamber-valve interactions (with ideal valve dynamics assumption) in multiple piston-chamber arrangements can be written as,

$$Q_a(\text{or } Q_{pcv,m}) = \underbrace{\underbrace{A_p \sum_{n=1}^{N_c} v_p\{2\pi f_p t + \phi_p\}}_{\text{multiple piston-chamber interaction}} \cdot \underbrace{F_n\{2\pi f_p t + \phi_p\} \cdot G_n\{2\pi f_p t + \phi_p - \phi_c\}}_{\text{ideal valve dynamics}}}_{\text{multiple piston-chamber-valve interaction}} \tag{A.7}$$

where the subscript pcv, m stands for piston-chamber-valve interaction in a multiple piston-chamber arrangements and Q_a the actual discharge pulsatile flow, $F_n = (1/2)(1 + \text{sign}(\sin(X_n)))$, $G_n = (1/2)(1 + \text{sign}(\sin(X_n - \phi_c)))$ and $X_n = 2\pi f_p t + 2\pi(n-1)/N_c$.

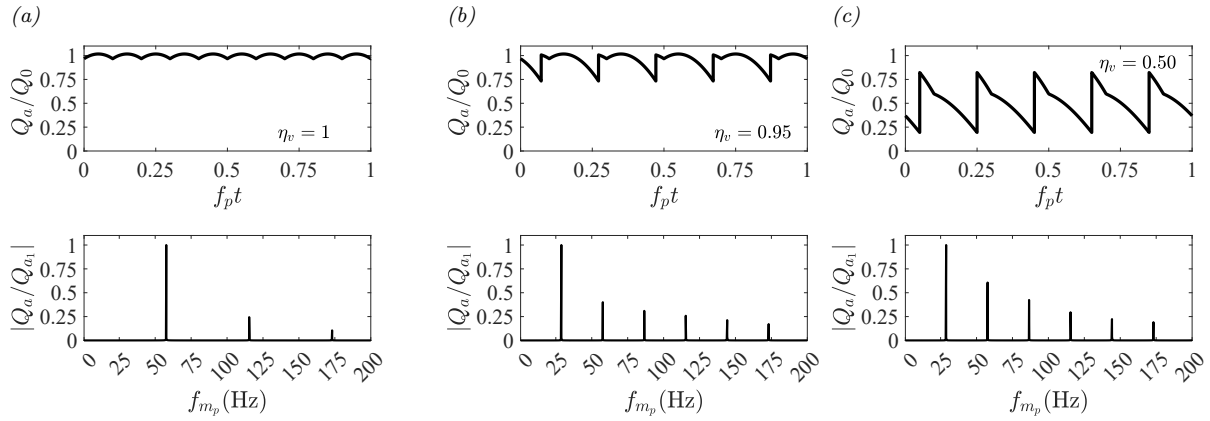

Figure A.8. Influence of volumetric efficiency (η_v) on the discharge pulsatile flow harmonics (Eq. 3) of a single five-chamber pump. The flows are plotted for a wide range of η_v under one crank rotation. The volume flux Q_a (y-axis) is normalised by mean flow Q_0 in time domain (top panel) and peak amplitude Q_{a_1} at the fundamental frequency in frequency-domain (bottom panel). Similar pulsatile flows in time-domain are plotted for pumps with three-chamber (triplex) in [45].

The pulsatile flow harmonics (Eq. 3) of Eq. (A.7) can be anticipated from the interaction mechanisms of piston kinematics, chamber fluid dynamics and valve dynamics – all together can be described in terms of volumetric efficiency (η_v). The volumetric efficiency of practical pumps is always less than unity ($\eta_v < 1$) due to the valve motion in a compressible liquid. This leads to distortion in the pulsatile flow profiles. To see how the high-pressure reciprocating pump influences the harmonics of pulsatile flow, we plotted the frequency spectrum of flows with a wide range of η_v (see Fig. A.8). It is clear that the fundamental frequency and harmonics of pulsatile flow are affected due to η_v.

Appendix B. Analytical derivation of the acoustic transmission line model

The dynamics of high-pressure unsteady flows in large piping networks can be encapsulated into compact low-dimensional mathematical models, ranging from zero-dimensional (0D) lumped-acoustic models to one-dimensional (1D) and two-dimensional (2D) distributed-acoustic models (linear, non-linear, compressible and incompressible) [50]. Here, we choose a 1D linear resistance compressible model in the frequency-domain to study the plane acoustic wave propagation in a pipe network.

Appendix B.1. Frequency-domain transcendental model

The linear dynamics of a one-dimensional (1D) slightly compressible (see Appendix C.3) unsteady pipe flow is governed by the system of hyperbolic partial differential equations (the continuity and momentum equations) [22, Chapter 2] as,

$$\frac{\partial p}{\partial t} + \frac{\rho_0 a_0^2}{A}\frac{\partial Q}{\partial s} = 0, \qquad \frac{\partial Q}{\partial t} + \frac{A}{\rho_0}\frac{\partial p}{\partial s} + \frac{\pi D}{\rho_0}\tau = 0, \tag{B.1}$$

where p is the cross-sectional averaged pressure, Q the cross-sectional averaged volume flux (or acoustic volume velocity), D the pipe inner diameter, A the pipe cross-sectional area, ρ_0 the mean fluid density at ambient condition, a_0 the speed of sound, s the spatial coordinate along the pipe centerline and τ the pipe wall shear stress. By combining mass and momentum equations in Eq.

B.1, the general linearised 1D acoustic wave propagation model in terms of volume flux Q can be written as,

$$\frac{\partial^2 Q}{\partial t^2} = a_0^2 \frac{\partial^2 Q}{\partial s^2} - \frac{\pi D}{\rho_0} \frac{\partial \tau}{\partial t}. \tag{B.2}$$

The 1D pipe wall shear shear stress is assumed linear, i.e. the τ can be expressed using convolution operation on Q as $\tau = \bar{\tau} * Q$ (where $\bar{\tau}$ is the linear approximation of shear stress) [28]. Applying Fourier transform to the Eq. (B.2) (assuming harmonic flow, i.e., $Q = \tilde{Q}(i\omega)e^{i\omega t}$) in a straight pipe element (j-k) leads to,

$$\frac{d^2 \tilde{Q}}{ds^2} = \underbrace{\left(\frac{-\omega^2}{a_0^2} + \frac{\pi D}{\rho_0 a_0^2} \tilde{\bar{\tau}} \right)}_{\Gamma_{jk}^2} \tilde{Q}, \tag{B.3}$$

where $\tilde{Q}(i\omega)$ and $\tilde{\bar{\tau}}$ are the Fourier transformed volume flux and Fourier transformed linear approximated shear stress, respectively. The solution of Eq. (B.3) can be written as,

$$\tilde{Q} = c_1 \sinh \Gamma_{jk} s + c_2 \cosh \Gamma_{jk} s, \tag{B.4}$$

where c_1 and c_2 are arbitrary constants. Assuming harmonic pressure, i.e., $p = \tilde{P}(i\omega)e^{i\omega t}$, and substituting Eq. (B.4) into the continuity equation (Eq. B.1) gives,

$$\tilde{P} = \frac{\rho_0 a_0^2 \Gamma_{jk}}{A i\omega} \big(c_1 \cosh \Gamma_{jk} s - c_2 \sinh \Gamma_{jk} s \big). \tag{B.5}$$

The constants (c_1 and c_2) can be determined from the flow conditions at indices j and k of pipe element. At pipe index j, i.e., $s = 0$, $\tilde{Q} = \tilde{Q}_{jk,j}$ and $\tilde{P} = \tilde{P}_j$. Eq. (B.4) and (B.5) gives,

$$c_1 = -\frac{A i\omega}{\rho_0 a_0^2 \Gamma_{jk}} \tilde{P}_j, \qquad c_2 = Q_{jk,j}. \tag{B.6}$$

At pipe index k, i.e, $s = L_{jk}$, $\tilde{Q} = \tilde{Q}_{jk,k}$ and $\tilde{P} = \tilde{P}_k$. Substituting theses values along with c_1 and c_2 into Eq. (B.4) and (B.5) gives,

$$\tilde{Q}_{jk,k} = \big(\cosh \Gamma_{jk} L_{jk} \big) \tilde{Q}_{jk,j} - \frac{1}{Z_c} \big(\sinh \Gamma_{jk} L_{jk} \big) \tilde{P}_j, \tag{B.7}$$

$$\tilde{P}_k = -Z_c \big(\sinh \Gamma_{jk} L_{jk} \big) \tilde{Q}_{jk,j} + \big(\cosh \Gamma_{jk} L_{jk} \big) \tilde{P}_j. \tag{B.8}$$

The matrix form of Eqs. B.7 and B.8 can be written as,

$$\begin{pmatrix} \tilde{Q}_{jk,k}(i\omega) \\ \tilde{P}_k(i\omega) \end{pmatrix} = \begin{pmatrix} \cosh\big(\Gamma_{jk}(i\omega) L_{jk}\big) & -Z_{c,jk}^{-1}(i\omega) \cdot \sinh\big(\Gamma_{jk}(i\omega) L_{jk}\big) \\ -Z_{c,jk}(i\omega) \cdot \sinh\big(\Gamma_{jk}(i\omega) L_{jk}\big) & \cosh\big(\Gamma_{jk}(i\omega) L_{jk}\big) \end{pmatrix} \begin{pmatrix} \tilde{Q}_{jk,j}(i\omega) \\ \tilde{P}_j(i\omega) \end{pmatrix}, \tag{B.9}$$

with the propagation operator $\Gamma_{jk}(i\omega)$ (see Eq. B.3) and characteristic impedance $Z_{c,jk}$,

$$\Gamma_{jk} = \frac{i\omega}{a_0} \sqrt{1 + \frac{\pi D}{\rho_0} \frac{\tilde{\bar{\tau}}}{i\omega}}, \qquad Z_{c,jk} = \frac{\rho_0 a_0}{A} \sqrt{1 + \frac{\pi D}{\rho_0} \frac{\tilde{\bar{\tau}}}{i\omega}}. \tag{B.10}$$

Appendix C. Justification of assumptions

Appendix C.1. Ideal valve dynamics

The ideal valve dynamics of the pump is considered in the piston-chamber-valve interaction mechanism. The ideal valve assumption suppresses the overshoot at the jump-discontinuity in the pulsatile flow (see Appendix A.3 and Fig. 1*b* and A.7*b*) [8].

Appendix C.2. Fluid is slightly compressible

The assumption of slightly compressible liquid ($|\partial\rho|/\rho_0 \ll 1$) means that the spatial variation of density is negligible. The density can be replaced with the mean (ambient) density ρ_0 in the equation of state [50] as,

$$\frac{\partial\rho}{\rho_0} = \frac{\partial p}{K} \qquad \Rightarrow \qquad a_0^2 = \frac{\partial p}{\partial\rho} = \frac{K}{\rho_0}, \tag{C.1}$$

By assuming liquid as slightly compressible, the small effect of density can be explicitly incorporated into the continuity equation via a constant value of the speed of sound in liquid $a_0(=(K/\rho_0)^{1/2})$. The continuity equation in terms of speed of sound is described in [Eq. B.1]. This assumption is valid for low-Mach number pipe flows.

Appendix C.3. Pipe walls are quasi-rigid

The acoustic waves propagates along the pipeline with a reduced wave propagation speed [22, Chapter 2] as,

$$a = \frac{a_0}{\sqrt{1+(K/E)\psi}}, \tag{C.2}$$

that depends on the speed of sound in liquid ($a_0 = (K/\rho_0)^{1/2}$ (where K is the liquid bulk modulus, ρ_0 the liquid density), the pipe Young's modulus (E) and pipe wall thickness and constraints (described in terms of ψ). The non-dimensionlised parameter ψ depends on the pipe material and geometrical properties and also on the external constraints (type of supports). For thick-walled elastic pipes [22, Chapter 2],

$$\psi = 2(1+\mu)\left(\frac{D_o^2+D^2}{D_o^2-D^2} - \frac{2\mu D^2}{D_o^2-D^2}\right), \tag{C.3}$$

where μ is the Poisson's ratio. On substituting values $\mu = 0.3$ (for steel), and pipe diameters (inner D and outer D_o) of a piping network (see Fig. 4*a* and 5*a*, listed in 4.1), $K = 2.1\times10^3$MPa (for water) and $E = 200\times10^3$MPa (for steel) into Eq. C.3, the non-dimensionlised parameter becomes $(K/E)\psi \simeq 0$. The wave propagation speed then reduces to $a \to a_0(=1480\text{m/s})$ [23], and pipe walls can be considered quasi-rigid.

Appendix C.4. Pipe flow model is linear

The assumption of the linear pipe flow model means that the advection terms are negligible, i.e.,

$$\frac{Q}{A}\frac{\partial Q}{\partial s} \ll \frac{\partial Q}{\partial t}. \tag{C.4}$$

The advection and acceleration terms can be scaled as,

$$Q\frac{\partial Q}{\partial s} \sim \frac{|Q_0|^2}{L} \quad \text{and} \quad \frac{\partial Q}{\partial t} \sim \frac{|Q_0|}{L/a_0}, \tag{C.5}$$

where Q_0 is the characteristic volume flux, L the characteristic length. In this study, the value of mean flow is Q_0 is $6.11 \times 10^{-3}\text{m}^3/\text{s}$ and wave propagation speed is $a_0 = 1480\text{m/s}$. Hence,

$$|Q_0|/A \sim 0.6 \ll a_0. \tag{C.6}$$

As the acoustic velocity (a_0) is significantly larger than the mean flow ($|Q_0|/A$), the momentum (advection) terms can be neglected.

Appendix C.5. Pipe flow model is one-dimensional

In one-dimensional (1D) pipe flow, the streamwise component of flow and pressure is assumed to be constant over the pipe cross-section [51]. The 1D pipe flow model in a slightly-compressible liquid-filled piping network means that the acoustic wave propagates as plane fronts along a network. The assumption of plane wave propagation is valid when the acoustic response is below the cut-off frequency $f_{\text{cut-off}} = 0.59a_0/D$ [52, Eq. 3.16, p. 105]. In this study, the pulsatile flow harmonics are significantly lower than the cut-off frequency ($f_{m_p} \ll f_{\text{cut-off}}$) and the plane acoustic wave is assumed accordingly.

Appendix C.6. Energy losses are one-dimensional and quasi-linear

The effect of losses on plane acoustic wave propagation in a piping network can be encapsulated into a pipe flow model using pipe wall shear stress models [50]. The approximation of instantaneous wall shear stress $\tau = \bar{\tau} * Q$ (where $\bar{\tau}$ is the linearised shear stress) [28] means that the loss is proportional to the mean flow. The contribution of instantaneous velocity profiles over pipe cross-section on the wall shear stress (τ) can be indirectly (not explicitly) modelled in terms of equivalent linear 1D velocities using: (a) the Darcy-Weisbach friction model for quasi-steady shear stress (τ_s) and (b) the convolution integral [33, 34, 35, 36] and instantaneous acceleration-based [53] methods for unsteady shear stress (τ_u) . We have adopted the convolution integral for unsteady shear stress formulation (see Eq. 6) in turbulent pipe flows, which is based on the Boussinesq hypothesis of a two-region, piecewise-linear, frozen eddy-viscosity distribution over a pipe cross-section.

Appendix D. Acoustic-turbulence interaction

During acoustic wave propagation in smooth-walled turbulent pipe flows, the boundary layer is comprised of two regions: (a) acoustic boundary layer with thickness $\delta_A = (2\nu/\omega)^{1/2}$ and (b) turbulent viscous sublayer with thickness $\delta_S = 5\nu/u_{\tau s}$ [54] (where $u_\tau = (\tau_s/\rho_o)^{1/2}$ is the mean friction velocity and τ_s the mean (steady) wall shear stress [55]). The contribution of turbulent effects on the acoustic attenuation depends on the relative length scales of the boundary layer present in the pipe flow, expressed in terms of non-dimensionalised acoustc boundary layer thickness [54, 56],

$$\delta_A^+ (= 5\delta_A/\delta_S) = \sqrt{\frac{2u_{\tau_s}^2}{\nu\omega}}. \tag{D.1}$$

The plane acoustic waves strongly attenuate when the acoustic boundary layer is thicker than the viscous sublayer ($\delta_A^+ \gg 1$) [54, 56, 57, 58, 59]. However, the turbulent mean flow has relatively thin acoustic boundary layer ($\delta_A^+ \lesssim 1$) in the practical industrial systems of high-frequency limit. The small δ_A^+ means that vorticity diffuses faster from the pipe wall and dies out before undergoing turbulent diffusion and the system behaves as quasi-laminar [54].

Pipe region	Pipe length L_s(m)	Pipe diameter D(m)	Fitting types	Fitting configuration	Number of fittings N_f	Equivalent length L_{eq}/D	$(1/D)\sum L_{eq}$
1-2	26.9	0.086	Bends	90-degree, $R_c/D = 2.3$	11	11	121
			Junctions	Flow-thru branch	1	60	60
			Valves	Globe valve, full open	3	320	960
2-3	21.5	0.086	Bends	90-degree, $R_c/D = 2.3$	11	11	121
			Junctions	Flow-thru branch	1	60	60
			Valves	Globe valve, full open	3	320	960
4-5	20.6	0.086	Bends	90-degree, $R_c/D = 2.3$	11	11	121
			Junctions	Flow-thru branch	1	60	60
			Valves	Globe valve, full open	3	320	960
4-6	39.7	0.111	Bends	90-degree, $R_c/D = 1.8$	11	11	121
			Junctions	Flow-thru branch	-	-	-
			Valves	Globe valve, full open	3	320	960

Table E.1. Configuration of pipe fittings in a piping network (see Fig. 4*a*) with equivalent lengths (L_{eq}) listed for each type of fittings in various segments of a network. The spatial dimension of the straight sections of each segment of a network (1-2, 2-3, 4-5 and 4-6) is also listed. Note: (a) R_c/D is the curvature ratio (where R_c is the bend radius of curvature), (b) the value of L_{eq} for valves is for fully-opened configuration, (c) a globe valve is associated with large energy loss even in fully-opened configuration and (d) the empirically-derived L_{eq}/D values are based on the new commercial steel pipe with absolute roughness $\epsilon = 0.045 \times 10^{-3}$m.

Appendix E. Fitting loss

The energy losses through piping networks can be categorised into major and minor (or local) losses. The major losses are associated with the fluid friction effects and the roughness of the wall in straight pipes, while the minor losses account for flow disturbances due to pipe fittings [60]. The term minor loss is a misnomer because the impact of minor losses can also be significant, e.g., valves even with fully-opened configurations [61] and a large number of pipe bends [62] and junctions [63] in a piping network generates large amount of energy losses [64, Chapter 1]. To avoid the confusion, we have adopted the term fitting losses instead of minor losses. The two ways to approximately integrate fitting losses into the pipe wall shear stress (Eq. 6) using empirically-based models are [65]: (a) the equivalent length (L_{eq}/D) method and (b) the resistance coefficient (K) method,

$$\underbrace{\tau_s = \frac{1}{8}\frac{\rho_0}{A^2}\underbrace{\left(\lambda + \lambda\sum_{n=1}^{N_f}\frac{L_{eq,n}}{L_s}\right)}_{\lambda+\lambda_{\text{fittings}}}|Q|Q,}_{\text{equivalent length method}} \quad \text{or} \quad \underbrace{\tau_s = \frac{1}{8}\frac{\rho_0}{A^2}\underbrace{\left(\lambda + D\sum_{n=1}^{N_f}\frac{K_n}{L_s}\right)}_{\lambda+\lambda_{\text{fittings}}}|Q|Q,}_{\text{resistance coefficient method}} \tag{E.1}$$

where λ and $\lambda_{\text{fittings}}$ are the quasi-steady friction loss factor associated with straight and fitting pipes, respectively; L_{eq} the equivalent length of pipe fittings, L_s the length of straight pipe components, N_f the number of various types of pipe fittings and $K = (L_{eq}/D)\lambda$. The equivalent length method assumes that pipe fittings can be replaced with the equivalent straight pipes that would have the same loss for same volume flux. The fitting equivalent length (L_{eq}) and fitting loss coefficient (K) depend on the flow regime (Re_0), type of fittings, number of fittings and spacing between the fittings [60, 61]. $\lambda = 0.025$ for rough-walled pipe with $\epsilon = 0.045 \times 10^{-3}$m.

Table E.1 shows the specification of pipe fittings involved in a piping network (see Fig. 4*a*). The various types of fittings in a network are bends, junctions and valves, which are distributed throughout the network. Each segment of the network (1-2, 2-3, 4-5 and 4-6) has eleven bends, one junction and three valves. To account for the losses due to fittings in a simplified three-branched network (see Fig. 5*a*), we first collected the equivalent lengths for each type of fittings from [60, 61]

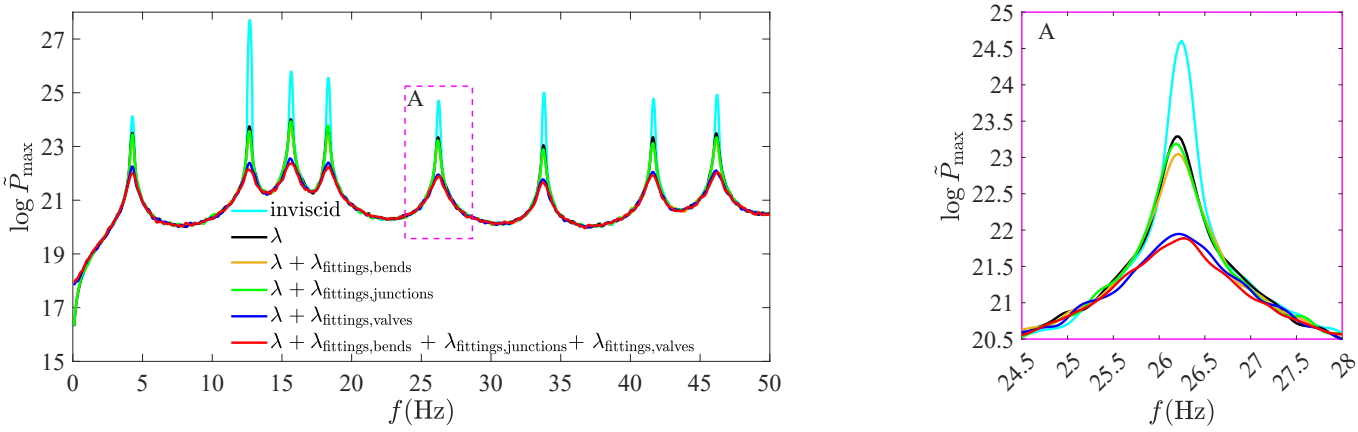

Figure E.9. Influence of fitting losses on the plane acoustic wave attenuation in a piping network (see Fig. 4*a* and 5*a*) in turbulent flow regime. The quasi-steady friction loss factor (λ) (Eq. 8) accounts the losses due to straight pipes. The quasi-steady fitting loss factors ($\lambda_{\text{fittings,bends}}$, $\lambda_{\text{fittings,junctions}}$ and $\lambda_{\text{fittings,valves}}$) (Eq. E.1) accounts the losses due to pipe fittings (listed in Table E.1), i.e., bends (48 in total), junctions (3 in total) and valves (9 in total), respectively. The zoomed-in plot of the fifth mode (region A) highlights the relative contribution of each type of fittings on the plane acoustic wave attenuation.

(or from the standard industrial handbooks). Each bend, junction and valve has an energy loss equivalent of 11, 60 and 320 pipe-diameter length of straight pipe. The quasi-steady fitting losses ($\lambda_{\text{fittings}}$) based on the equivalent length method are then estimated. Similar to Fig. 4*b* under random flow excitation, the responses of a network are captured for each type of pipe fittings. Figure E.9 shows the contribution of loss factor for straight and fitting pipes on the plane acoustic wave attenuation. It is clear that the losses associated with pipe fittings have a significant effect on the plane acoustic wave attenuation. The attenuation due to fitting losses depends on the number and types of fittings. The greater plane acoustic wave attenuation associated with valves compared with bends and junctions can be anticipated from the large pressure drop through the long equivalent lengths of globe valves.

References

[1] M. L. Munjal, Acoustics of ducts and mufflers with application to exhaust and ventilation system design, John Wiley & Sons, 1987. URL: https://books.google.co.uk/books/about/Acoustics_of_Ducts_and_Mufflers_With_App.html?id=Z-s50vk-U68C.

[2] P. Gao, J. Zhai, Q. Han, Dynamic response analysis of aero hydraulic pipeline system under pump fluid pressure fluctuation, Proc. Inst. Mech. Eng., Part G: J. Aero. Eng. 233 (2019) 1585–1595. URL: https://doi.org/10.1177%2F0954410018756697.

[3] A. Maekawa, T. Tsuji, M. Noda, T. Takahashi, M. Kato, K. Fujita, Experimental and numerical study on pressure pulsations under various acoustic boundary conditions in piping systems, J. Press. Vess. Tech. 139 (2017). URL: https://doi.org/10.1115/1.4035698.

[4] API-688, Pulsation and vibration control in positive displacement machinery systems for petroleum, petrochemical, and natural gas industry services, A. Petrol. Inst. 1 (2012) 1–128. URL: https://global.ihs.com/doc_detail.cfm?document_name=API%20RP%20688&item_s_key=00585664.

[5] EI, Guidelines for the avoidance of vibration induced fatigue failure in process pipe work, Energy Institute, London 2 (2008). URL: https://www.google.co.uk/books/edition/Guidelines_for_the_Avoidance_of_Vibratio/wDOjAQAACAAJ?hl=en.

[6] K. Edge, D. Tilley, The use of plane wave theory in the modelling of pressure ripples in hydraulic systems, Trans. Inst. Meas., Control 5 (1983) 171–178. URL: https://doi.org/10.1177%2F014233128300500401.

[7] T. Nakamura, S. Kaneko, F. Inada, M. Kato, K. Ishihara, T. Nishihara, N. W. Mureithi, M. A. Langthjem, Flow-induced vibrations: classifications and lessons from practical experiences, second ed., Butterworth-Heinemann, 2013. URL: https://doi.org/10.1016/C2011-0-07518-X.

[8] P. J. Singh, N. K. Madavan, Complete analysis and simulation of reciprocating pumps including system piping, in: Proc. 4th Intl. Pump Users Symp., 1987, pp. 55–74. URL: http://oaktrust.library.tamu.edu/handle/1969.1/164308.

[9] W. W. Parry, System problem experience in multiple reciprocating pump installations, in: Proc. 3rd Intl. Pump Users Symp., 1986, pp. 21–25. URL: https://oaktrust.library.tamu.edu/handle/1969.1/164340.

[10] Y. Zeng, Z. Yao, F. Wang, R. Xiao, C. He, Experimental and numerical investigations of vibration characteristics induced by pressure fluctuations in a parallel operating pumping system, J. Hyd. Eng. 147 (2021) 04021020. URL: https://doi.org/10.1061/(ASCE)HY.1943-7900.0001894.

[11] A. Brighenti, F. Bittante, R. Parrozzani, Advanced simulation techniques, Hydro Eng. 14 (2009) 103–106. URL: https://www.researchgate.net/publication/298565128_Advanced_simulation_techiques.

[12] C. W. S. To, The acoustic simulation and analysis of complicated reciprocating compressor piping systems, I: Analysis technique and parameter matrices of acoustic elements, J. Sound Vib. 96 (1984) 175–194. URL: https://doi.org/10.1016/0022-460X(84)90577-7.

[13] M. L. Munjal, A. G. Doige, On uniqueness, transfer and combination of acoustic sources in one-dimensional systems, J. Sound Vib. 121 (1988) 25–35. URL: https://doi.org/10.1016/S0022-460X(88)80058-0.

[14] J. Lavrentjev, M. Åbom, Characterization of fluid machines as acoustic multi-port sources, J. Sound Vib. 197 (1996) 1–16. URL: https://doi.org/10.1006/jsvi.1996.0514.

[15] G. Mikota, B. Manhartsgruber, F. Hammerle, A. Brandl, Hydraulic modal analysis in theory and practice, Trans. ASME: J. Dyn. Sys., Meas., Control 141 (2019) 051007. URL: https://doi.org/10.1115/1.4042145.

[16] A. Snakowska, J. Jurkiewicz, A new approach to the theory of acoustic multi-port networks with multimode wave and its application to muffler analysis, J. Sound Vib. 490 (2021) 115722. URL: https://doi.org/10.1016/j.jsv.2020.115722.

[17] T. Fujikawa, M. Kato, H. Ito, H. Nomura, A method of estimating pulsation response of a piping system driven by two reciprocating compressors, in: JSME: Proc. C., volume 55, 1989, pp. 904–909. URL: https://doi.org/10.1299/kikaic.55.904.

[18] J. E. Miller, The reciprocating pump: theory, design, and use, John Wiley & Sons, 1987. URL: https://www.amazon.co.uk/Reciprocating-Pump-Theory-Design-Use/dp/0471854670.

[19] H. H. Tackett, J. A. Cripe, G. Dyson, Positive displacement reciprocating pump fundamentals-power and direct acting types, in: Proc. 24th Intl. Pump Users Symp., 2008. URL: https://oaktrust.library.tamu.edu/handle/1969.1/163923.

[20] G. Vetter, F. Schweinfurther, Pressure pulsations in the piping of reciprocating pumps, Chem. Eng. Technol. 10 (1987) 262–271. URL: https://doi.org/10.1002/ceat.270100132.

[21] ANSYS, Ansys mechanical APDL acoustic analysis guide, Canonsburg, ANSYS Inc, USA (2013).

[22] M. H. Chaudhry, Applied hydraulic transients, Springer, 1979. URL: https://link.springer.com/book/10.1007/978-1-4614-8538-4.

[23] E. B. Wylie, V. L. Streeter, L. Suo, Fluid transients in systems, volume 1, Prentice Hall Englewood Cliffs, NJ, 1993. URL: https://books.google.co.uk/books/about/Fluid_Transients_in_Systems.html?id=Ep9RAAAAMAAJ&redir_esc=y.

[24] A. F. D'Souza, R. Oldenburger, Dynamic response of fluid lines, J. Basic Eng. 86 (1964) 589–598. URL: https://doi.org/10.1115/1.3653180.

[25] E. B. Wylie, Resonance in pressurized piping systems, Trans. ASME: J. Basic Eng. 87 (1965) 960–966. URL: https://doi.org/10.1115/1.3650851.

[26] M. H. Chaudhry, Resonance in pressurized piping systems, J. Hydraulics Div. 96 (1970) 1819–1839. URL: https://doi.org/10.1061/JYCEAJ.0002680.

[27] A. C. Zecchin, A. R. Simpson, M. F. Lambert, L. B. White, J. P. Vítkovskỳ, Transient modeling of arbitrary pipe networks by a laplace-domain admittance matrix, J. Eng. Mech. 135 (2009) 538–547. URL: https://doi.org/10.1061/(ASCE)0733-9399(2009)135:6(538).

[28] A. C. Zecchin, M. F. Lambert, A. R. Simpson, L. B. White, Frequency-domain modeling of transients in pipe networks with compound nodes using a laplace-domain admittance matrix, J. Hydraulic Eng. 136 (2010) 739–755. URL: https://doi.org/10.1061/(ASCE)HY.1943-7900.0000248.

[29] G. Mikota, B. Manhartsgruber, H. Kogler, F. Hammerle, Modal testing of hydraulic pipeline systems, J. Sound Vib. 409 (2017) 256–273. URL: https://doi.org/10.1016/j.jsv.2017.08.001.

[30] H. F. Duan, T. C. Che, P. J. Lee, M. S. Ghidaoui, Influence of nonlinear turbulent friction on the system frequency response in transient pipe flow modelling and analysis, J. Hydraulic Res. 56 (2018) 451–463. URL: https://doi.org/10.1080/00221686.2017.1399936.

[31] J. P. Vítkovskỳ, P. J. Lee, A. C. Zecchin, A. R. Simpson, M. F. Lambert, Head-and flow-based formulations for frequency domain analysis of fluid transients in arbitrary pipe networks, Journal of Hydraulic Engineering 137 (2011) 556–568. URL: https://doi.org/10.1061/(ASCE)HY.1943-7900.0000338.

[32] W. Zielke, Frequency-dependent friction in transient pipe flow, Trans. ASME: J. Basic Eng. 90 (1968) 109–115. URL: https://doi.org/10.1115/1.3605049.

[33] A. E. Vardy, J. M. Brown, Transient, turbulent, smooth pipe friction, J. Hydraulic Res. 33 (1995) 435–456. URL: https://doi.org/10.1080/00221689509498654.

[34] A. E. Vardy, J. M. Brown, Transient turbulent friction in smooth pipe flows, J. Sound Vib. 259 (2003) 1011–1036. URL: https://doi.org/10.1006/jsvi.2002.5160.

[35] A. E. Vardy, J. M. Brown, Transient turbulent friction in fully rough pipe flows, J. Sound Vib. 270 (2004) 233–257. URL: https://doi.org/10.1016/S0022-460X(03)00492-9.

[36] A. E. Vardy, J. M. Brown, Approximation of turbulent wall shear stresses in highly transient pipe flows, J. Hydraulic Eng. 133 (2007) 1219–1228. URL: https://doi.org/10.1061/(ASCE)0733-9429(2007)133:11(1219).

[37] H. Duan, S. Meniconi, P. Lee, B. Brunone, M. S. Ghidaoui, Local and integral energy-based evaluation for the unsteady friction relevance in transient pipe flows, J. Hydraulic Eng. 143 (2017) 04017015. URL: http://dx.doi.org/10.1061/(ASCE)HY.1943-7900.0001304.

[38] A. Adamkowski, M. Lewandowski, Experimental examination of unsteady friction models for transient pipe flow simulation, Trans. ASME: J. Fluids Eng. 128 (2006) 1351–1363. URL: https://doi.org/10.1115/1.2354521.

[39] H. F. Duan, M. S. Ghidaoui, P. J. Lee, Y. K. Tung, Relevance of unsteady friction to pipe size and length in pipe fluid transients, J. Hdraulic Eng. 138 (2012) 154–166. URL: http://dx.doi.org/10.1061/(ASCE)HY.1943-7900.0000497.

[40] R. Von Bernuth, Simple and accurate friction loss equation for plastic pipe, J. Irrigation Drainage Eng. 116 (1990) 294–298. URL: https://doi.org/10.1061/(ASCE)0733-9437(1990)116:2(294).

[41] Y. A. Cengel, Fluid mechanics, Tata McGraw-Hill Education, 2013. URL: https://www.google.co.uk/books/edition/Fluid_Mechanics_Fundamentals_and_Applica/PeZSlAEACAAJ?hl=en.

[42] F. W. Williams, S. Yuan, K. Ye, D. Kennedy, M. S. Djoudi, Towards deep and simple understanding of the transcendental eigenproblem of structural vibrations, J. Sound Vib. 256 (2002) 681–693. URL: https://doi.org/10.1006/jsvi.2002.5016.

[43] L. E. Kinsler, A. R. Frey, A. B. Coppens, J. V. Sanders, Fundamentals of acoustics, Whiley, 1999. URL: https://www.wiley.com/en-gb/Fundamentals+of+Acoustics,+4th+Edition-p-9780471847892.

[44] COMSOL, The acoustics module user's guide, 2017. URL: https://doc.comsol.com/5.3/doc/com.comsol.help.aco/AcousticsModuleUsersGuide.pdf.

[45] G. Vetter, B. Seidl, Pressure pulsation dampening methods for reciprocating pumps, in: Proc. 10th Intl. Pump Users Symp., volume 19, 1993. URL: https://oaktrust.library.tamu.edu/handle/1969.1/164214.

[46] N. D. Manring, The discharge flow ripple of an axial-piston swash-plate type hydrostatic pump, Trans. ASME: J. Dyn. Syst. 122 (2000) 263–268. URL: https://doi.org/10.1115/1.482452.

[47] V. L. Streeter, E. B. Wylie, Hydraulic transients caused by reciprocating pumps, J. Eng. Power. 89 (1967) 615–620. URL: https://doi.org/10.1115/1.3616754.

[48] J. C. Wachel, S. M. Price, Understanding how pulsation accumulators work, in: Energy-Source Technol. Conference Exhibition, Houston, Texas, 1988, pp. 23–31. URL: https://engdyn.com/resources/understanding-how-pulsation-accumulators-work/.

[49] A. Josifovic, J. Corney, B. Davies, Valve dynamics in multi-cylinder positive displacement pump model, in: IEEE Intl. Conf. Adv. Int. Mechatronics, IEEE, 2015, pp. 35–41. URL: https://doi.org/10.1109/AIM.2015.7222505.

[50] J. S. Stecki, D. C. Davis, Fluid transmission lines—distributed parameter models part 1: A review of the state of the art, Proc. Inst. Mech. Eng., Part A: Power Proc. Eng. 200 (1986) 215–228. URL: https://doi.org/10.1243%2FPIME_PROC_1986_200_032_02.

[51] F. Ahmed, I. Eames, E. Moeendarbary, E. Azarbadegan, High-strouhal-number pulsatile flow in a curved pipe, J. Fluid Mech. 923 (2021) A15,1–28. URL: https://doi.org/10.1017/jfm.2021.553.

[52] C. Q. Howard, B. S. Cazzolato, Acoustic analyses using MATLAB and ANSYS, CRC press, 2014. URL: https://uk.mathworks.com/academia/books/acoustic-analyses-using-matlab-and-ansys-howard.html.

[53] B. Brunone, U. M. Golia, M. Greco, Effects of two-dimensionality on pipe transients modeling, J. Hydraulic Eng. 121 (1995) 906–912. URL: https://doi.org/10.1061/(ASCE)0733-9429(1995)121:12(906).

[54] C. Weng, A. Hanifi, S. Boij, Sound-turbulence interaction in low mach number duct flow, in: 19th AIAA/CEAS Aeroacoustics Conf., 2013, p. 2024. URL: https://doi.org/10.2514/6.2013-2024.

[55] Y. Kita, Y. Adachi, K. Hirose, Periodically oscillating turbulent flow in a pipe, JSME Bulletin 23 (1980) 656–664. URL: https://doi.org/10.1299/jsme1958.23.656.

[56] D. Ronneberger, C. Ahrens, Wall shear stress caused by small amplitude perturbations of turbulent boundary-layer flow: an experimental investigation, J. Fluid Mech. 83 (1977) 433–464. URL: https://doi.org/10.1017/S0022112077001281.

[57] M. Howe, The damping of sound by wall turbulent shear layers, J.Acoust. Soc. Am. 98 (1995) 1723–1730. URL: https://doi.org/10.1121/1.414408.

[58] S. Allam, M. Åbom, Investigation of damping and radiation using full plane wave decomposition in ducts, J. Sound Vib. 292 (2006) 519–534. URL: https://doi.org/10.1016/j.jsv.2005.08.016.

[59] E. Dokumaci, On attenuation of plane sound waves in turbulent mean flow, J. Sound Vib. 320 (2009) 1131–1136. URL: https://doi.org/10.1016/j.jsv.2008.09.002.

[60] D. S. Miller, Internal flow: A guide to losses in pipe and duct systems, British Hydromechanics Research Association, 1971. URL: https://books.google.co.uk/books/about/Internal_flow.html?id=hAjbAQAACAAJ&redir_esc=y.

[61] D. S. Miller, Internal flow systems, British Hydromechanics Research Association, 1978. URL: https://books.google.co.uk/books/about/Internal_Flow_Systems.html?id=8pJRAAAAMAAJ.

[62] M. Annan, E. A. Gooda, Effect of minor losses during steady flow in transmission pipelines–case study "water transmission system upgrade in northern saudi arabia", Alex. Eng. J. 57 (2018) 4299–4305. URL: https://doi.org/10.1016/j.aej.2018.12.002.

[63] D. J. Wood, L. S. Reddy, J. Funk, Modeling pipe networks dominated by junctions, Journal of Hydraulic Engineering 119 (1993) 949–958. URL: https://doi.org/10.1061/(ASCE)0733-9429(1993)119:8(949).

[64] J. P. Tullis, Hydraulics of pipelines: Pumps, valves, cavitation, transients, John Wiley & Sons, 1989. URL: https://books.google.co.uk/books?id=86P9PVgKXoEC&printsec=frontcover&redir_esc=y#v=onepage&q&f=false.

[65] D. W. Wood, T. Walters, Operational problems in pumping non-settling slurries resolved using an improved laminar flow pipe fitting loss model, in: Proc. 28th Intl. Pump Users Symp., 2012. URL: https://oaktrust.library.tamu.edu/handle/1969.1/162574.